

# Universal bounds on current fluctuations

Patrick Pietzonka,<sup>1</sup> Andre C. Barato,<sup>2</sup> and Udo Seifert<sup>1</sup>

<sup>1</sup>*II. Institut für Theoretische Physik, Universität Stuttgart, 70550 Stuttgart, Germany*

<sup>2</sup>*Max Planck Institute for the Physics of Complex Systems, Nöthnitzer Straße 38, 01187 Dresden, Germany*

For current fluctuations in non-equilibrium steady states of Markovian processes, we derive four different universal bounds valid beyond the Gaussian regime. Different variants of these bounds apply to either the entropy change or any individual current, e.g., the rate of substrate consumption in a chemical reaction or the electron current in an electronic device. The bounds vary with respect to their degree of universality and tightness. A universal parabolic bound on the generating function of an arbitrary current depends solely on the average entropy production. A second, stronger bound requires knowledge both of the thermodynamic forces that drive the system and of the topology of the network of states. These two bounds are conjectures based on extensive numerics. An exponential bound that depends only on the average entropy production and the average number of transitions per time is rigorously proved. This bound has no obvious relation to the parabolic bound but it is typically tighter further away from equilibrium. An asymptotic bound that depends on the specific transition rates and becomes tight for large fluctuations is also derived. This bound allows for the prediction of the asymptotic growth of the generating function. Even though our results are restricted to networks with a finite number of states, we show that the parabolic bound is also valid for three paradigmatic examples of driven diffusive systems for which the generating function can be calculated using the additivity principle. Our bounds provide a new general class of constraints for nonequilibrium systems.

PACS numbers: 05.70.Ln, 05.40.-a

## I. INTRODUCTION

Equilibrium statistical physics is governed by a universal principle stating that in an isolated system each microstate is equally likely. For a system in contact with a heat bath, thus the famous Gibbs-Boltzmann distribution arises that involves only the Hamiltonian of the system and the temperature of the bath. In non-equilibrium, a similarly universal principle is not known and may not even exist. One characteristic feature of non-equilibrium systems is that they necessarily come with dissipation, i.e., entropy production. Non-equilibrium steady states, generated by time-independent driving have a constant average entropy production. Observed for a finite time, the entropy change exhibits fluctuations that are universally constrained by the fluctuation theorem [1–6], which is arguably the most universal principle discovered for non-equilibrium systems so far.

The fluctuation theorem relates the probability to observe a negative entropy change to the one for observing the corresponding positive value. In this sense, it constrains “half” of the distribution. Experiments have illustrated and tested this symmetry, *inter alia*, for colloidal particles [7–9], energy exchange between two conductors [10], small electronic systems at low temperature [11], molecular motors [12], and shaken granular matter [13–15]. In a refined version, the fluctuation theorem holds not only for entropy change but also for the joint probability of all currents contributing to the entropy change [5, 16], which involves the corresponding affinities like non-conservative forces for colloids, chemical potential differences for bio-molecular reactions or

voltage drops for electronic circuits. Generally, these individual currents in a multi-cyclic network, however, are not restricted by the fluctuation theorem or any other universal result.

In this paper, we introduce a complementary class of constraints, not only on the distribution of entropy change, but of any individual current in a network. These constraints universally bound the fluctuations over the full range of positive and negative values, in particular the extreme fluctuations. The crucial parameters characterizing these bounds are the average entropy production, the affinities, topological features like the number of states in a cycle and the activity, i.e., the average number of transitions per unit time. If one knows such parameters, current fluctuations can be bounded independently of the specific transition rates. Correspondingly, a measurement of such current fluctuations will make it possible to infer constraints on these parameters which in an experiment may not be known or not be directly accessible. This study substantially extends and generalizes work in which we have recently explored universal relations between dissipation and dispersion of currents leading to a general thermodynamic uncertainty relation [17] and allowing the inference of topological properties of enzymatic networks [18, 19].

We employ the formalism of large deviations [20, 21] in which for large times the exponential decay of the tails of the distribution function is characterized by a rate function. This rate function can be obtained from the Legendre transformation of the scaled cumulant generating function. For the latter, we derive a series of lower bounds that can be divided into four classes: a parabolic

bound, a hyperbolic cosine bound, an exponential bound, and an asymptotic bound relevant for large values of  $z$ , where  $z$  is the real variable in the scaled cumulant generating function. The last two bounds can be proved exactly while the first two are conjectures based on extensive numerics. These universal bounds are valid for any nonequilibrium system described by a Markov process with a finite number of states.

The hydrodynamic fluctuation theory for driven diffusive systems in contact with two reservoirs by Bertini *et al.* [22–24] has been another major development in nonequilibrium statistical physics. This theory leads to a (typically hard) variational problem that, if solved, leads to the exact rate function of the current of particles or heat between reservoirs. The additivity principle derived in [25] is a more direct method that allows for the calculation of the scaled cumulant generating function related to the current in driven diffusive systems. For example, this method has been used to calculate this function for the symmetric simple exclusion process (SSEP) [25, 26], the Kipnis-Marchioro-Pressuti (KMP) model [27, 28], and the weakly asymmetric simple exclusion process (WASEP) [29]. These results are valid in the limit of large system size, for which the number of states diverges. Even though our bounds are restricted to the case of a finite number of states, we show that the scaled cumulant generating functions obtained from the additivity principle for these three models lies inside our parabolic bound.

The paper is divided as follows. In Sec. II we define the entropy, the currents and their generating functions. Our main results are summarized in Sec. III. Secs. IV, V, VI, and VII contain the parabolic, hyperbolic cosine, exponential, and asymptotic bounds, respectively. In Sec. VIII, the parabolic bound is compared with exact results for the SSEP, the KMP model, and the WASEP. We conclude in Sec. IX. The appendices contain various proofs and details on the numerics.

## II. LARGE DEVIATIONS IN MARKOVIAN NETWORKS

We consider a Markovian network consisting of  $N$  discrete states  $\{i\}$  and allow for transitions with rates  $k_{ij} \geq 0$  from state  $i$  to  $j$ . All transitions are taken to be reversible, i.e.,  $k_{ij} > 0$  implies  $k_{ji} > 0$ . The time dependent probability distribution  $p_i(t)$  of state  $i$  at time  $t$  evolves according to the master equation

$$\partial_t p_i(t) = \sum_j \mathcal{L}_{ij} p_j(t) \equiv \sum_j [k_{ji} - r_i \delta_{ij}] p_j(t), \quad (1)$$

where the exit rate from state  $i$  is defined as

$$r_i \equiv \sum_\ell k_{i\ell}. \quad (2)$$

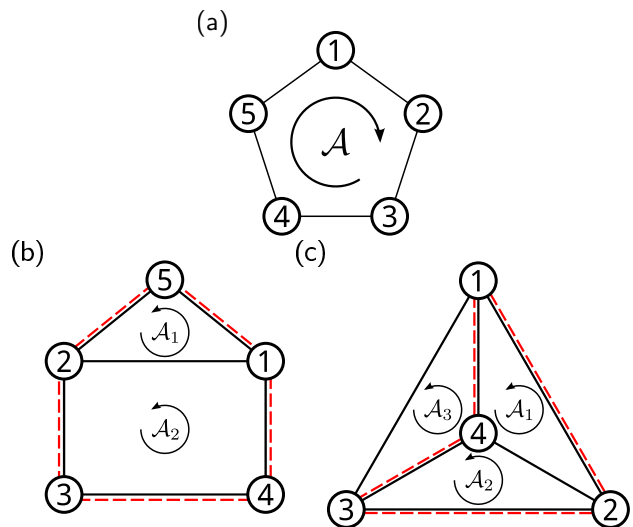


FIG. 1. (a) Unicyclic network with affinity  $\mathcal{A}$  and five states. (b) Multicyclic network with two fundamental cycles, one with three states and affinity  $\mathcal{A}_1$  and the other with four states and affinity  $\mathcal{A}_2$ . The red dashed lines indicate a cycle with affinity  $\mathcal{A}_1 + \mathcal{A}_2$  and five states. (c) Multicyclic network with three fundamental cycles with three states each. The affinities of these cycles are  $\mathcal{A}_1$ ,  $\mathcal{A}_2$ , and  $\mathcal{A}_3$ . The red dashed lines indicate a cycle with affinity  $\mathcal{A}_1 + \mathcal{A}_2$  and four states.

For large times  $t$ ,  $p_i(t)$  tends to the stationary distribution  $p_i^s$ , which satisfies  $\sum_j \mathcal{L}_{ij} p_i^s = 0$ .

Following Schnakenberg, we identify a complete set of fundamental cycles  $\{\beta\}$  within the network [30]. Each cycle is associated with an affinity  $\mathcal{A}_\beta$ , a fluctuating current  $X_\beta(t)$  that counts cycle completions after time  $t$  (the so-called *integrated current*) and an average current

$$J_\beta \equiv \langle X_\beta(t) \rangle / t, \quad (3)$$

where the brackets indicate an average over stochastic trajectories. The average is independent of  $t$  for initial conditions drawn from the steady state distribution.

Upon a transition  $i \rightarrow j$ ,  $X_\beta$  increases by the generalized distance  $d_{ij}^\beta = -d_{ji}^\beta$ . These increments are constrained to add up to one for every closed loop that completes the cycle once in forward direction. For example,  $X_\beta$  could be the scaled displacement of a molecular motor. The affinity  $\mathcal{A}_\beta$  would then be given by the external force times the length of a full motor step, while  $d_{ij}^\beta$  denotes the relative length of a sub-step related to the conformational change  $i \rightarrow j$ . The ratio of forward and backward transition rates fulfill the local detailed balance relation

$$\ln(k_{ij}/k_{ji}) = \sum_\beta d_{ij}^\beta \mathcal{A}_\beta + E_i - E_j, \quad (4)$$

where  $E_i$  denotes the equilibrium free energy associated with state  $i$ , and, in general, the sum over  $\beta$  is a sum over all fundamental cycles in the network of states [30]

(see also [16, 31] for a precise definition of a fundamental cycle). For notational convenience we have set Boltzmann's constant  $k_B$  and the temperature  $T$  to unity, thus energies and affinities are given in units of the thermal energy  $k_B T$ . The (fluctuating) entropy change in the surrounding medium  $s_m(t)$  is given by the increments  $d_{ij}^s = \ln(k_{ij}/k_{ji})$ . The average entropy production reads

$$\sigma \equiv \langle s_m(t) \rangle / t = \sum_{\beta} \mathcal{A}_{\beta} J_{\beta}. \quad (5)$$

Adopting a vector notation  $\mathbf{X}$  for the set of all cycle currents  $X_{\beta}$  the scaled cumulant generating function is defined as

$$\lambda(\mathbf{z}) \equiv \lim_{t \rightarrow \infty} \frac{1}{t} \ln \langle \exp[\mathbf{z} \cdot \mathbf{X}(t)] \rangle, \quad (6)$$

where  $\mathbf{z}$  is a real vector. As an abbreviation we will refer to  $\lambda(\mathbf{z})$  simply as the ‘‘generating function’’. It can be shown that  $\lambda(\mathbf{z})$  is the largest eigenvalue of the modified Markov generator  $\mathcal{L}_{ij}(\mathbf{z})$ , which is defined as [5, 32]

$$\mathcal{L}_{ij}(\mathbf{z}) \equiv \mathcal{L}_{ij} \exp(\mathbf{z} \cdot \mathbf{d}_{ji}), \quad (7)$$

where  $\mathbf{d}_{ji}$  is a vector with components  $d_{ji}^{\beta}$ . The variable  $X_{\beta}/t$ , or more conveniently the scaled variable

$$\xi_{\beta} \equiv X_{\beta}/(tJ_{\beta}), \quad (8)$$

satisfies a large deviation principle [21, 33] of the form

$$\text{Prob}(\mathbf{X}, t) \sim \exp[-th(\boldsymbol{\xi})] \quad (9)$$

with a rate function  $h(\boldsymbol{\xi})$  that is given by the Legendre-Fenchel transform

$$h(\boldsymbol{\xi}) = \max_{\mathbf{z}} \left[ \sum_{\beta} z_{\beta} J_{\beta} \xi_{\beta} - \lambda(\mathbf{z}) \right]. \quad (10)$$

The fluctuation theorem is a symmetry, known as Gallavotti-Cohen symmetry, on the generating function of the form [5, 16]

$$\lambda(\mathbf{z}) = \lambda(-\mathcal{A} - \mathbf{z}). \quad (11)$$

In terms of the rate function this symmetry reads

$$-h(\boldsymbol{\xi}) + h(-\boldsymbol{\xi}) = \sum_{\beta} \xi_{\beta} J_{\beta} \mathcal{A}_{\beta}. \quad (12)$$

The generating function related to a single fluctuating current  $X_{\alpha}$  is

$$\lambda_{\alpha}(z) \equiv \lambda(z\mathbf{e}_{\alpha}) = \lim_{t \rightarrow \infty} \frac{1}{t} \ln \langle \exp[zX_{\alpha}(t)] \rangle, \quad (13)$$

where  $\mathbf{e}_{\alpha}$  is the unit vector associated with the current in cycle  $\alpha$ . Generally, this function does not exhibit a symmetry of the form (11) as extensively discussed in

[31] (see also [34, 35]). In contrast, the evaluation of  $\lambda(\mathbf{z})$  along the vector  $\mathcal{A}$  yields

$$\lambda_s(z) \equiv \lambda(z\mathcal{A}) = \lim_{t \rightarrow \infty} \frac{1}{t} \ln \langle \exp[zs_m(t)] \rangle \quad (14)$$

as the generating function of the entropy change. It is symmetric with respect to  $z = -1/2$ , which expresses the fluctuation theorem that holds for this observable. The rate functions associated with the probability distributions of these variables read

$$h_{\alpha}(\xi_{\alpha}) = \max_z [zJ_{\alpha}\xi_{\alpha} - \lambda_{\alpha}(z)] \quad (15)$$

and, introducing the scaled entropy change  $s \equiv s_m(t)/(\sigma t)$  in analogy to Eq. (8),

$$h_s(s) = \max_z [z\sigma s - \lambda_s(z)], \quad (16)$$

respectively.

An important distinction in this paper is the one between unicyclic and multicyclic networks of states, illustrated in Fig. 1. For unicyclic networks, where there is only a single affinity  $\mathcal{A} \equiv \mathcal{A}_{\alpha}$  and a single fluctuating current  $X \equiv X_{\alpha}$ , we no longer have to distinguish between the different types of generating functions and can simply write

$$\lambda(z) \equiv \lambda_{\alpha}(z) = \lambda_s(z/\mathcal{A}). \quad (17)$$

In the following, we will be interested in functions  $b(z)$  that bound the generating function  $\lambda(z)$  from below, i.e.,

$$b(z) \leq \lambda(z) \quad (18)$$

for all  $z$ . As special cases, the relation (18) can be used to extract bounds for individual fluctuating currents,  $\lambda_{\alpha}(z) \geq b_{\alpha}(z) \equiv b(z\mathbf{e}_{\alpha})$ , and the entropy change,  $\lambda_s(z) \geq b_s(z) \equiv b(z\mathcal{A})$ . Such bounds immediately imply upper bounds on the rate functions

$$h_{\alpha}(\xi_{\alpha}) \leq \max_z [zJ_{\alpha}\xi_{\alpha} - b_{\alpha}(z)]. \quad (19)$$

and

$$h_s(s) \leq \max_z [z\sigma s - b_s(z)]. \quad (20)$$

For any generating function the coefficients of the Taylor expansion around  $z = 0$  correspond to the cumulants. The Fano factor that quantifies the dispersion of the distribution is defined as

$$F \equiv \lim_{t \rightarrow \infty} \frac{\langle X(t)^2 \rangle - \langle X(t) \rangle^2}{\langle X(t) \rangle} = \frac{\lambda''(0)}{\lambda'(0)}, \quad (21)$$

where  $X$  is a random variable. We denote the Fano factor associated with an individual current by  $F_{\alpha}$  and the one associated with the entropy change in the medium by  $F_s$ . Since global lower bounds  $b(z)$  with  $b(0) = 0$  must share

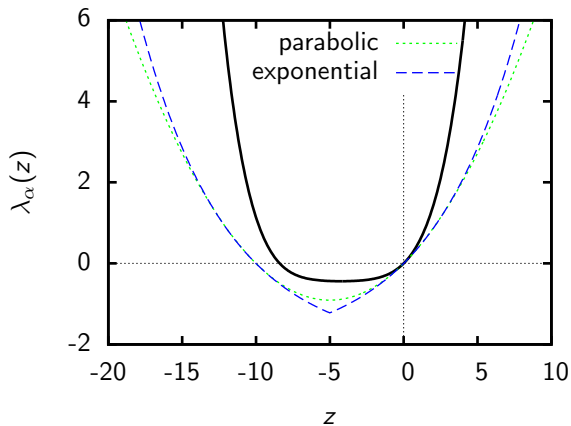


FIG. 2. Illustration of our two main results for the generating function of an individual cycle current (thick black curve). The parabolic bound that depends on the entropy production is shown as a green dotted line and the exponential bound that depends on the entropy production and the activity is shown as a blue dashed line. The generating function refers to the cycle  $\alpha = 1$  of the “house-shaped” network shown in Fig. 1b. The affinities are  $\mathcal{A}_1 = 8$  and  $\mathcal{A}_2 = 6$ , all transition rates were set to 1 except for  $k_{15} = \exp(\mathcal{A}_1/2)$ ,  $k_{51} = \exp(-\mathcal{A}_1/2)$ ,  $k_{41} = \exp(\mathcal{A}_2/2)$ , and  $k_{14} = \exp(-\mathcal{A}_2/2)$ . The quantities relevant for the bounds are the average current  $J_\alpha \simeq 0.36$ , the entropy production  $\sigma \simeq 3.6$ , and the activity  $R \simeq 2.13$ .

a tangent with  $\lambda(z)$  at  $z = 0$  while having a stronger curvature, every such bound implies with

$$F \geq \frac{b''(0)}{b'(0)} \quad (22)$$

a bound on the Fano factor.

Since  $\lambda(0) = 0$  holds trivially for all networks, we usually require that our bounds are saturated for  $z = 0$ . This requirement will only be lifted for a bound that captures the asymptotic behavior for large  $|z|$  in Sec. VII. Hence, if  $\lambda(z)$  is analytic,  $b(z)$  must have the same gradient as  $\lambda(z)$ .

### III. SUMMARY OF MAIN RESULTS

The two main bounds on the generating function obtained in this paper are illustrated in Fig. 2. First, the generating function  $\lambda(z)$  for any network is bounded by a parabola according to

$$\lambda(z) \geq z \cdot \mathbf{J} (1 + z \cdot \mathbf{J}/\sigma). \quad (23)$$

This parabolic bound depends only on the average entropy production. Second,  $\lambda(z)$  is also bounded from below by an exponential function of the form

$$\lambda(z) \geq R \left[ e^{(|\sigma/2 + z \cdot \mathbf{J}| - \sigma/2)/R} - 1 \right]. \quad (24)$$

This second bound depends on the average entropy production and on the activity  $R \equiv \sum_i p_i^s r_i$ , which is the

average number of transitions per time in the whole network.

Choosing a specific direction for the vector  $z$ , both bounds are valid both for any individual fluctuating current and for the entropy change. It is quite remarkable that the fluctuations of any current in an arbitrary multicyclic network can be bounded by a function involving only the average entropy production in the case of the parabolic bound and the average entropy production and activity in the case of the exponential bound. Even though there is no obvious relation between the parabolic bound and the exponential bound, typically, the exponential bound becomes tighter than the parabolic bound both for far from equilibrium conditions and for large  $|z|$ .

We derive two further relevant lower bounds on  $\lambda(z)$  in this paper. (1) A hyperbolic cosine bound, which is an extension of the parabolic bound that is tighter and requires further knowledge of the affinities and the topology of the network. (2) An asymptotic bound that becomes tight for large values of  $|z|$  and requires knowledge of all transition rates.

These bounds are complementary to the fluctuation theorem. Whereas they establish the minimal value that  $\lambda(z)$  can take, the fluctuation theorem constrains  $\lambda(z)$  to have the symmetry (11).

## IV. PARABOLIC BOUND

### A. Linear response regime

In the limit of small affinities  $\mathcal{A}_\beta$ , the average current  $J_\alpha$  depends linearly on the affinities,

$$J_\alpha = \sum_\beta L_{\alpha\beta} \mathcal{A}_\beta \quad (25)$$

with the symmetric and positive definite Onsager matrix  $L_{\alpha\beta} \equiv \partial J_\alpha / \partial \mathcal{A}_\beta |_{\mathcal{A}=0}$ . In the region  $z \lesssim \mathcal{O}(\mathcal{A})$ , the generating function  $\lambda(z)$  can be expanded as a quadratic form around its center of symmetry, which is, due to Eq. (11), located at  $z = -\mathcal{A}/2$ . The requirement  $\lambda(0) = 0$  and  $\nabla \lambda(0) = \mathbf{J}$  fixes this expansion to

$$\lambda(z) = \sum_{\beta,\gamma} (z_\beta + \mathcal{A}_\beta/2) L_{\beta\gamma} (z_\gamma + \mathcal{A}_\gamma/2) - \sigma/4, \quad (26)$$

where the entropy production  $\sigma$  is given in Eq. (5). Evaluating this function for  $z = z e_\alpha$  yields as generating function related to the individual current

$$\lambda_\alpha(z) = z J_\alpha + z^2 L_{\alpha\alpha}. \quad (27)$$

The positive definiteness of the matrix  $G_{\beta\gamma} \equiv (L_{\alpha\alpha} L_{\beta\gamma} - L_{\alpha\beta} L_{\alpha\gamma})$  [36] (with  $\alpha$  fixed) yields

$$\sum_{\beta,\gamma} G_{\beta\gamma} \mathcal{A}_\beta \mathcal{A}_\gamma = L_{\alpha\alpha} \sigma - J_\alpha^2 \geq 0. \quad (28)$$

Hence  $\lambda_\alpha(z)$  is bounded from below by

$$\lambda_\alpha(z) \geq zJ_\alpha(1 + zJ_\alpha/\sigma). \quad (29)$$

Using the Legendre transform (19), this bound can be transformed into a bound for the rate function

$$h_\alpha(\xi_\alpha) = \frac{L_{\alpha\alpha}}{4J_\alpha^2}(\xi_\alpha - 1)^2 \leq \frac{\sigma}{4}(\xi_\alpha - 1)^2. \quad (30)$$

Since the direction  $\mathbf{e}_\alpha$  can be chosen arbitrarily, the bound (29) can be stated in a multidimensional formulation as

$$\lambda(\mathbf{z}) \geq \mathbf{z} \cdot \mathbf{J}(1 + \mathbf{z} \cdot \mathbf{J}/\sigma). \quad (31)$$

Equality holds along the line  $\mathbf{z} \propto \mathbf{A}$ , which corresponds to the generating function  $\lambda_s(z) = \lambda(\mathbf{A}z)$  associated with entropy change. Within linear response, the rate function for the scaled entropy change  $s$  is thus given by

$$h_s(s) = \frac{\sigma}{4}(s - 1)^2. \quad (32)$$

Eq. (30) shows that the knowledge of the average entropy production is sufficient to bound the whole range of fluctuations of any individual current in the linear response regime. Surprisingly, as we show next, this parabolic bound is also valid beyond the linear response regime.

The parabolic bound has also an important consequence for fluctuations in systems at equilibrium. To study this case it is more convenient to scale the fluctuating currents as  $x_\beta \equiv X_\beta/t = J_\beta \xi_\beta$ . For the corresponding rate function  $\tilde{h}_\alpha(x_\alpha) = h_\alpha(x_\alpha J_\alpha)$ , the bound (30) then reads

$$\tilde{h}_\alpha(x_\alpha) \leq \frac{1}{4} \frac{\sum_{\gamma\delta} L_{\gamma\delta} \mathcal{A}_\gamma \mathcal{A}_\delta}{\left(\sum_\beta L_{\alpha\beta} \mathcal{A}_\beta\right)^2} x_\alpha^2 + \mathcal{O}(\mathcal{A}), \quad (33)$$

for small  $\mathcal{A}_\beta$  with fixed  $x_\alpha$ . Here, we have represented the average currents using Eq. (25). This bound is supported by our numerics presented in appendix B as, where we have checked (29) also for  $\mathbf{z} \gtrsim \mathcal{O}(\mathbf{A})$ . For multicyclic networks at equilibrium, the prefactor in (33) depends on the direction in which the limit  $\mathbf{A} \rightarrow 0$  is taken. In particular, choosing  $\mathbf{A} \propto \mathbf{e}_\alpha$  yields

$$\tilde{h}_\alpha(x_\alpha) \leq x_\alpha^2/(4D_\alpha). \quad (34)$$

Thus, the equilibrium fluctuations of any current  $X_\alpha$  can be bounded by the parabola that is defined as the continuation of the quadratic expansion of the rate function around  $x_\alpha = 0$ . In other words, the Gaussian approximation for typical fluctuations always underestimates the probability of extreme fluctuations in equilibrium systems. Since this bound is exact for small  $x_\alpha$ , performing the limit  $\mathbf{A} \rightarrow 0$  in a direction different from  $\mathbf{e}_\alpha$  cannot yield a stronger bound.

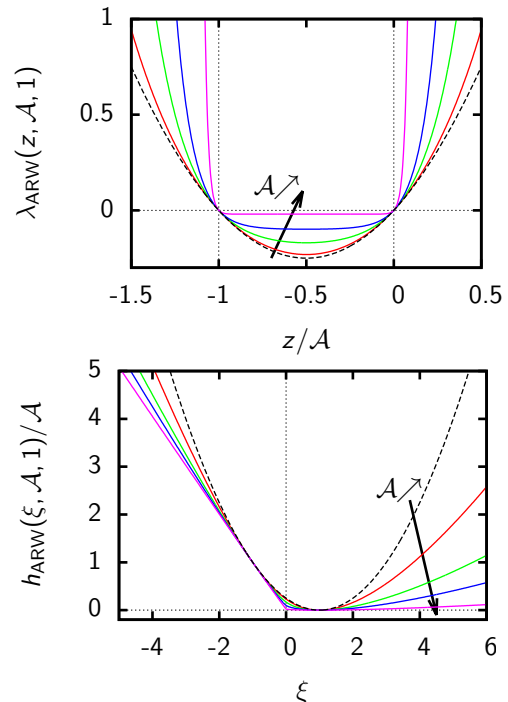


FIG. 3. The generating function  $\lambda(z)$  and the rate function  $h(\xi)$  of the asymmetric random walk for selected affinities  $\mathcal{A}$  (2, 5, 10, 50) and  $N = 1$ . Black arrows indicate the direction of increasing  $\mathcal{A}$ . The parabolic bound for the generating function (40) and for the rate function (41) are shown as black dashed curves.

## B. Beyond linear response: Unicyclic case

The parabolic shape of the generating function for  $z \lesssim \mathcal{O}(\mathcal{A})$  and of the rate function for  $\xi \lesssim \mathcal{O}(1)$  can be regarded as a signature of linear response. It arises only for nearly vanishing affinities or for freely diffusing particles, where the linearity between affinity and current persists even for high affinities. Beyond this regime, one universally observes two characteristic changes in the rate function [37–39]. First, the tails for large values of  $|\xi_\alpha|$  grow no longer quadratically but with a scaling somewhere between linear and quadratic. Second, there is a formation of a “kink” around the value  $\xi_\alpha = 0$ . For finite numbers of states, the rate function is still analytic in this region, but it exhibits a significantly enhanced curvature. In the Legendre transformed picture of the generating function  $\lambda_\alpha(z)$ , these two effects show up as a faster than quadratic growth for large  $z$  and a pronounced plateau around the minimum of  $\lambda_\alpha(z)$ .

This behavior of the generating function is best illustrated with an asymmetric random walk (ARW), as shown in Fig. 3. Consider a network consisting of a single cycle with  $N$  vertices and affinity  $\mathcal{A}$ , as shown in Fig. 1a. The hopping rates in forward and backward directions  $k^+$  and  $k^-$  are uniform with

$$\ln \frac{k^+}{k^-} = \mathcal{A}/N. \quad (35)$$

The average current in this model is  $J = (k^+ - k^-)/N$  and the entropy production is  $\sigma = J\mathcal{A}$ . It can be shown that the generating function is given by [5]

$$\begin{aligned}\lambda(z) &= k^+ \left[ e^{z/N} + e^{-(z+\mathcal{A})/N} - 1 - e^{-\mathcal{A}/N} \right] \\ &= J\lambda_{\text{ARW}}(z, \mathcal{A}, N),\end{aligned}\quad (36)$$

where

$$\lambda_{\text{ARW}}(z, \mathcal{A}, N) \equiv \frac{\cosh[(z + \mathcal{A}/2)/N] - \cosh[\mathcal{A}/(2N)]}{(1/N) \sinh[\mathcal{A}/(2N)]}.\quad (37)$$

Similarly, the rate function corresponding to the generating function (36) is given by [5]

$$h(\xi) = J h_{\text{ARW}}(\xi, \mathcal{A}, N),\quad (38)$$

where

$$\begin{aligned}h_{\text{ARW}}(\xi, \mathcal{A}, N) &\equiv \frac{N}{\sinh[\mathcal{A}/(2N)]} \left[ a\xi \operatorname{arsinh}(a\xi) - a\xi \frac{\mathcal{A}}{2N} \right. \\ &\quad \left. - \sqrt{1 + (a\xi)^2} + \sqrt{1 + a^2} \right]\end{aligned}\quad (39)$$

and  $a \equiv \sinh[\mathcal{A}/(2N)]$ . As shown in Fig. 3, the generating function (36) is bounded from below by the parabola

$$\lambda_{\text{ARW}}(z, \mathcal{A}, N) \geq zJ(1 + z/\mathcal{A}),\quad (40)$$

and the rate function is bounded from above by the parabola

$$h_{\text{ARW}}(z, \mathcal{A}, N) \leq \mathcal{A}(\xi - 1)^2/4.\quad (41)$$

In Sec. V, we will show in the context of an even stronger, affinity-dependent bound, that the bound (40) holds also for arbitrary unicyclic networks with non-uniform transition rates.

### C. Beyond linear response: multicyclic case

Based on numerical evidence we conjecture that

$$\lambda(z) \geq z \cdot \mathbf{J} (1 + z \cdot \mathbf{J}/\sigma)\quad (42)$$

holds globally for all vectors  $\mathbf{z}$  and for all types of Markovian networks. In terms of the individual current in a cycle  $\alpha$ , this conjecture can be formulated as

$$\lambda_\alpha(z) \geq zJ_\alpha(1 + zJ_\alpha/\sigma)\quad (43)$$

whereas for the entropy change

$$\lambda_s(z) \geq z\sigma(1 + z).\quad (44)$$

The bound (42) becomes the same as (31) in the linear response regime. However, (42) is also valid beyond this regime where the currents  $\mathbf{J}$  are the actual average

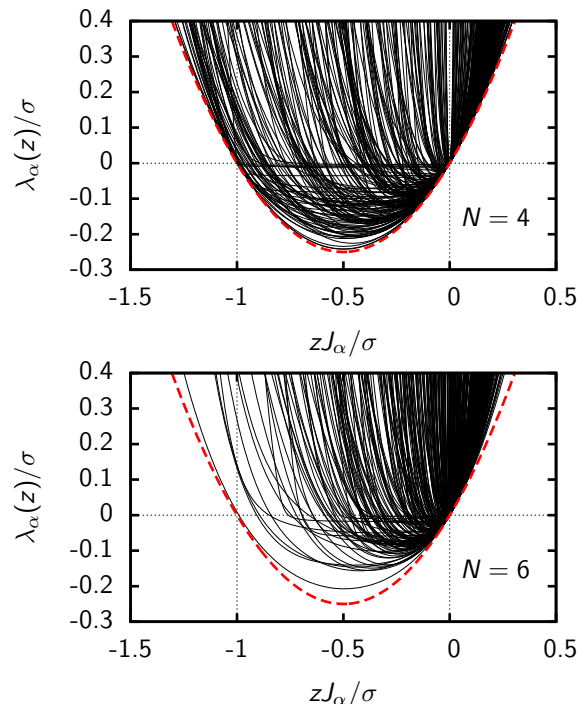


FIG. 4. Generating functions  $\lambda_\alpha(z)$  for an individual current in fully connected networks with random transition rates. The black curves in the upper and lower panels correspond to networks with  $N = 4$  and  $N = 6$  vertices, respectively. The parabolic bound (43) is shown as a dashed curve.

currents in the steady state, as determined from  $\nabla\lambda(0)$ , which are different from the linear response currents (25).

The numerical evidence for this bound is illustrated in Fig. 4. We generated a large set of networks of states with random transition rates, drawn according to the procedure described in appendix B. As the affinity increases, generating functions globally deviate in a positive direction from the parabolic shape. Only at the trivial points  $z = 0$  and  $z = -\mathcal{A}$  does the generating function in Eq. (42) acquire with zero the same value for all networks. For larger networks ( $N = 6$ ) the left hand side of the plot becomes less populated, since the probability of the vectors  $\mathbf{e}_\alpha$  and  $\mathcal{A}$  being nearly parallel becomes smaller in higher dimensions. The full numerical evidence for this parabolic bound is explained in appendix B.

The local evaluation (22) of the parabolic bound (43) for an individual current yields the relation

$$F_\alpha\sigma/J_\alpha \geq 2\quad (45)$$

for the Fano factor associated with the current  $X_\alpha$ . This “thermodynamic uncertainty relation”, which imposes a minimal energetic cost that must be paid for small uncertainty in the output of an enzymatic reaction, has been derived in [17]. Hence, the parabolic bound is a generalization of this relation. From relation (45), measurements of the dispersion and average of an individual current can provide a lower bound on the average entropy production

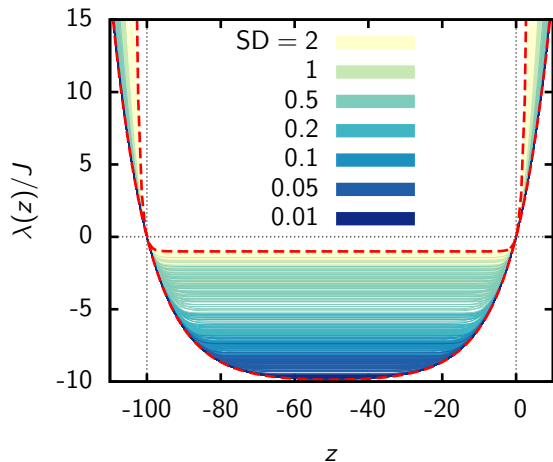


FIG. 5. Generating function  $\lambda(z)$  scaled by the steady state current  $J$  in unicyclic networks with  $N = 10$  states and fixed affinity  $\mathcal{A} = 100$ . The gray-scale (color-scale) encodes the standard deviation (SD) used for sampling the transition rates (see appendix B). Dark gray (blue) corresponds to a nearly uniform distribution of transition rates and light gray (yellow) to a broad distribution of transition rates. The lower and upper bounds (50) and (51), respectively, are shown as (red) dashed lines.

$\sigma \geq 2J_\alpha/F_\alpha$ . This bound makes it possible to estimate the entropy production by measuring a single individual current [40, 41]. Applied to the entropy production in the medium, the parabolic bound (44) leads to

$$F_s \geq 2. \quad (46)$$

## V. HYPERBOLIC COSINE BOUND

### A. Unicyclic networks

For a unicyclic network, the parabolic bound is saturated in the linear response regime. As shown in Fig. 3 for the asymmetric random walk, the generating function deviates more from the parabolic bound as the affinity  $\mathcal{A}$  increases. We now discuss an affinity dependent bound that is stronger than the parabolic bound. This affinity dependent bound is also less universal as it requires the knowledge of  $\mathcal{A}$ . For example, in a biochemical network a fixed affinity means that the chemical potential difference driving a chemical reaction is known.

The transition rates for an arbitrary unicyclic model with  $N$  states and periodic boundary conditions are denoted by

$$k_{i,i+1} = k_i^+ \text{ and } k_{i,i-1} = k_i^-, \quad (47)$$

where  $i = 1, 2, \dots, N$ . A fixed affinity  $\mathcal{A}$  implies the constraint

$$\frac{\prod_{i=1}^N k_i^+}{\prod_{i=1}^N k_i^-} = e^{\mathcal{A}} \quad (48)$$

on the transition rates. Different choices of the transition rates that fulfill this restriction can lead to different generating functions, as shown in Fig. 5. In particular, if the transition rates are uniform, i.e.,  $k_i^+ = k^+$  and  $k_i^- = k^-$  the generating function divided by the average current  $\lambda(z)/J$  becomes  $\lambda_{\text{ARW}}(z, \mathcal{A}, N)$ , which is given in Eq. (37). The opposite extreme choice for the transition rates is the case where the network behaves effectively like there was only one link between states ( $N = 1$ ) and all the affinity is concentrated in this single link. In this case  $\lambda(z)/J$  becomes  $\lambda_{\text{ARW}}(z, \mathcal{A}, 1)$ , which fulfills  $\lambda_{\text{ARW}}(z, \mathcal{A}, 1) \geq \lambda_{\text{ARW}}(z, \mathcal{A}, N)$ .

From these considerations we conjecture that for unicyclic networks

$$\lambda_{\text{ARW}}(z, \mathcal{A}, 1) \geq \lambda(z)/J \geq \lambda_{\text{ARW}}(z, \mathcal{A}, N). \quad (49)$$

Hence, using the definition (37), Eq. (49) implies the lower bound

$$\lambda(z) \geq J \frac{\cosh[(z + \mathcal{A}/2)/N] - \cosh[\mathcal{A}/(2N)]}{(1/N) \sinh[\mathcal{A}/(2N)]}, \quad (50)$$

which we call the hyperbolic cosine bound for a unicyclic network. This conjectured bound is supported by the numerical evidence shown in Fig. 5. Eq. (49) also leads to an upper bound

$$\lambda(z) \leq J \frac{\cosh(z + \mathcal{A}/2) - \cosh(\mathcal{A}/2)}{\sinh(\mathcal{A}/2)}. \quad (51)$$

A rigorous proof for this upper bound is provided in appendix C.

In Fig. 6, we show the bounds (50) and (51) for different values of the affinity. For smaller  $\mathcal{A}$  the bounds are closer to each other. In the linear response regime, up to quadratic order in  $z$ , they become the same and equal to the parabolic bound in Eq. (40).

The bounds in Eqs. (50) and (51) lead to the bounds

$$\coth\left(\frac{\mathcal{A}}{2}\right) \geq F \geq \frac{1}{N} \coth\left(\frac{\mathcal{A}}{2N}\right) \quad (52)$$

on the Fano factor defined in Eq. (22). The lower bound is an affinity dependent bound on the Fano factor that has been obtained in [17]. In the formal limit  $\mathcal{A} \rightarrow \infty$  it becomes  $F \geq 1/N$ . This bound for formally divergent affinity is a key result in statistical kinetics [42] as it allows for an estimate on the number of states  $N$  from measurements of the Fano factor. The upper bound on  $F$  in Eq. (52) is a new result. It is a generalization of the known result  $F \leq 1$ , which is also valid in the limit  $\mathcal{A} \rightarrow \infty$  [42].

For systems at equilibrium, the bounds (49) become

$$2D[\cosh(z) - 1] \geq \lambda(z) \geq 2DN^2[\cosh(z/N) - 1], \quad (53)$$

which is obtained using the linear response current  $J = D\mathcal{A}$  with the Einstein relation for the diffusion constant

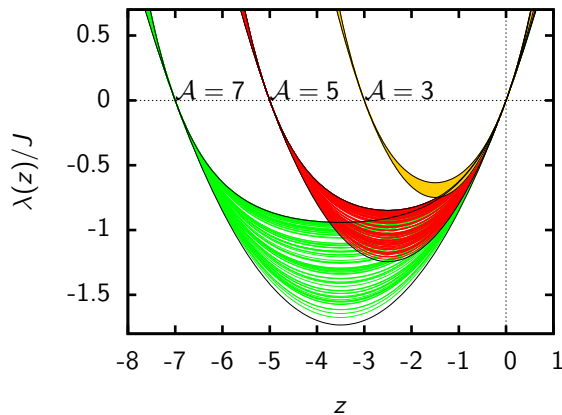


FIG. 6. Generating function  $\lambda(z)$  scaled by the steady state current  $J$  in unicyclic networks with  $N = 10$  for three families of distinct affinities  $\mathcal{A}$ . For each family, transition rates were sampled according to the procedure described in appendix B. The black curves refer to the lower and upper bound from Eqs. (50) and (51).

$D$  and letting  $\mathcal{A} \rightarrow 0$ . Thus, the bound (34) for the rate function of the variable  $x = X/t$  can be refined to

$$\tilde{h}(x) \leq N \left[ x \operatorname{arsinh} \left( \frac{x}{2DN} \right) + 2DN - \sqrt{x^2 + (2DN)^2} \right] \quad (54)$$

for unicyclic networks.

### B. Multicyclic networks

A formulation of an affinity dependent bound for multicyclic networks is more involved. In this case, the affinities of the fundamental cycles are fixed, which means that the transition rates are constrained by relations of the form (48) for each fundamental cycle. The hyperbolic cosine bound for the generating function of the entropy change reads

$$\lambda_s(z) \geq \sigma \frac{\cosh[(z + 1/2)\mathcal{A}^*/n^*] - \cosh[\mathcal{A}^*/(2n^*)]}{(\mathcal{A}^*/n^*) \sinh[\mathcal{A}^*/(2n^*)]}, \quad (55)$$

where the affinity  $\mathcal{A}^*$  and the number of states  $n^*$  corresponds to the smallest ratio  $\mathcal{A}/n$  among all the cycles in the network. We note that a local evaluation of the form (22) of the bound (55) leads to [18]

$$F_s \geq \frac{\mathcal{A}^*}{n^*} \coth \left( \frac{\mathcal{A}^*}{2n^*} \right). \quad (56)$$

This bound can be used to estimate the number of intermediate states in enzymatic schemes from measurements of the Fano factor in single molecule experiments, as discussed in [18].

In order to explain how to identify  $\mathcal{A}^*/n^*$  we consider the network of states in Fig. 1c. We arbitrarily choose the cycles (1, 4, 2, 1) with affinity  $\mathcal{A}_1$ , (2, 4, 3, 2) with affinity

$\mathcal{A}_2$ , and (1, 3, 4, 1) with affinity  $\mathcal{A}_3$  as the three fundamental cycles. Any other cycle in the network is just a composition of these fundamental cycles; for example, the cycle (1, 4, 3, 2, 1), which is marked with a red dotted line in Fig. 1c, with affinity  $\mathcal{A}_1 + \mathcal{A}_2$  is the sum of the first and second fundamental cycles. If the affinities are  $\mathcal{A} = (1, 2, 3)$  then the cycle with the smallest affinity per number of states is the fundamental cycle (1, 4, 2, 1). Therefore, in this case  $\mathcal{A}^* = 1$  and  $n^* = 3$ . If the affinities are  $\mathcal{A} = (-11, 12, 13)$ , where a negative affinity means that the direction of the current in the cycle with affinity  $\mathcal{A}_1$  in Fig. 1c changes from anti-clockwise to clockwise, the cycle with minimal affinity per number of states is (1, 4, 3, 2, 1). In this case  $\mathcal{A}^* = 1$  and  $n^* = 4$ .

The basic idea behind the bound in Eq. (55) is as follows. Given a network of states with fixed affinities, the transition rates that lead to the smallest possible  $\lambda_s(z)/J$  are those for which the cycle with smallest  $\mathcal{A}/n$  dominates the network. This cycle dominates the network if the transition rates within the cycle are large, transition rates to leave the cycle are small, and transition rates to return to the cycle are large. With this choice for the transition rates the multicyclic network is effectively a unicyclic network with affinity  $\mathcal{A}^*$  and number of states  $n^*$ , for which the bound (50) holds. Any other choice of rates will just add cycles with a smaller affinity per number of states, which cannot decrease fluctuations.

Our numerical evidence presented in Fig. 7d shows that this hyperbolic cosine bound is also valid for any individual current  $X_\alpha$  in the form

$$\lambda_\alpha(z) \geq \sigma \frac{\cosh[(zJ_\alpha/\sigma + 1/2)\mathcal{A}^*/n^*] - \cosh[\mathcal{A}^*/(2n^*)]}{(\mathcal{A}^*/n^*) \sinh[\mathcal{A}^*/(2n^*)]}. \quad (57)$$

Hence, the hyperbolic cosine bound can be written in the more general form

$$\lambda(z) \geq \sigma \frac{\cosh[(z \cdot \mathbf{J}/\sigma + 1/2)\mathcal{A}^*/n^*] - \cosh[\mathcal{A}^*/(2n^*)]}{(\mathcal{A}^*/n^*) \sinh[\mathcal{A}^*/(2n^*)]}. \quad (58)$$

The full numerical evidence for this conjecture is discussed in appendix B. If the cycle relevant for the bound (57) has a rather small affinity per number of states, which is often the case in a large network of states, the bound is only slightly stronger than the parabolic bound (43), as visible in Fig. 7a and 7c. An often tighter bound for this situation is derived in the next section. Our numerics indicates that an affinity dependent upper bound on the generating function in the multicyclic case does not exist. For fixed affinities, the generating function can become arbitrarily close to the trivial bound  $\lambda_s(z) < 0$  for  $-1 < z < 0$ , visible in Fig. 7a-c. A generalization of the equilibrium bound (54) to multicyclic networks is not directly possible, since the identification of a cycle with minimal  $\mathcal{A}/n$  becomes ambiguous in the limit  $\mathcal{A} \rightarrow 0$ .



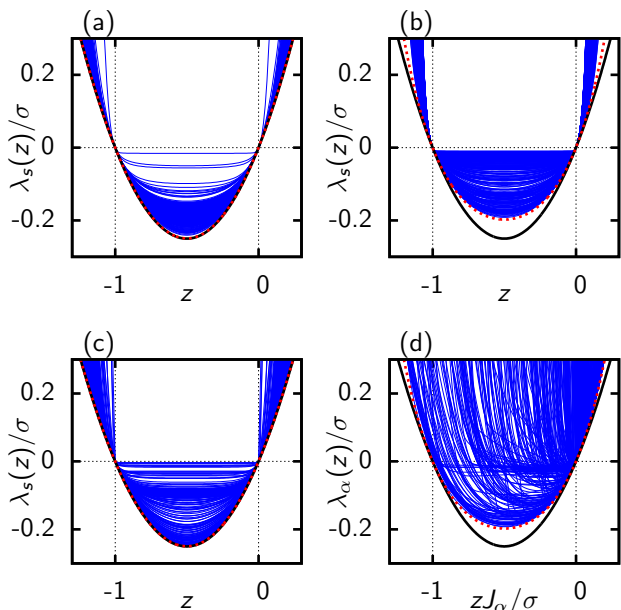


FIG. 7. Generating functions for entropy change (a-c) and randomly selected individual currents  $X_\alpha$  (d) for the network of Fig. 1c. The affinities are  $\mathcal{A} = (1, 2, 3)$  in (a),  $\mathcal{A} = (11, 12, 13)$  in (b) and (d), and  $\mathcal{A} = (-11, 12, 13)$  in (c). The black curves correspond to the parabolic bound and the red dashed curves correspond to the hyperbolic cosine bound. The generating functions were generated as explained in appendix B. In panel (a)  $\mathcal{A}^*/n^* = 1/3$ , in panels (b) and (d)  $\mathcal{A}^*/n^* = 11/3$ , and in panel (c)  $\mathcal{A}^*/n^* = 1/4$ . For small values of  $\mathcal{A}^*/n^*$ , as in panels (a) and (c), the parabolic and hyperbolic cosine bound are closer to each other.

## VI. EXPONENTIAL BOUND

A rigorous lower bound on the largest eigenvalue  $\lambda(\mathbf{z})$  of the matrix  $\mathcal{L}(\mathbf{z})$  can be obtained from the algebraic properties of positive matrices. Specifically, a remarkable theorem about the largest eigenvalue  $\mu$  of an arbitrary matrix with non-negative entries  $B_{ij}$  from Ellis [20, Theorem IX.4.4] is

$$\ln \mu = \sup_{\tau_{ij}} \sum_{i,j} \tau_{ij} \ln \frac{B_{ij} \nu_i}{\tau_{ij}}, \quad (59)$$

where  $\nu_i \equiv \sum_{\ell} \tau_{i\ell}$  and  $0 \ln 0 \equiv 0$ . The admissible matrices  $\tau_{ij}$  must satisfy certain normalization and symmetry properties given in appendix A. For any specific matrix  $\tau_{ij}$ , Eq. (59) provides a lower bound on  $\mu$ .

In order to apply Eq. (59) to the modified Markov generator  $\mathcal{L}_{ij}(\mathbf{z})$ , we construct a positive matrix

$$B_{ij}(\mathbf{z}) \equiv \delta_{ij} + \eta \mathcal{L}_{ij}(\mathbf{z}) \quad (60)$$

with a sufficiently small parameter  $\eta > 0$ . Its largest eigenvalue is given by  $1 + \eta \lambda(\mathbf{z})$ . Making use of the known eigenvector of  $\mathcal{L}_{ij}(0)$ , which is the stationary distribution  $p_i^s$ , we can choose  $\tau_{ij}$  such that the supremum (59) is saturated for  $\mathbf{z} = 0$ . As we show in appendix A, fixing

this choice for all values of  $\mathbf{z}$ , Eq. (59) yields the bound

$$\lambda(\mathbf{z}) \geq (e^{\eta \mathbf{z} \cdot \mathbf{J}} - 1)/\eta \quad (61)$$

on the generating function.

The largest possible  $\eta$  in Eq. (60) provides the strongest bound. The maximal value that still complies with the requirement for a non-negative entries  $B_{ij}$  is the inverse of the maximal exit rate  $\eta = 1/\max_i(r_i)$ . Extending the proof of Eq. (59) in appendix A, we can show that Eq. (61) is valid for larger values of  $\eta$  up to

$$\eta = 1/R \quad (62)$$

where

$$R \equiv \sum_i p_i^s r_i \leq \max_i r_i, \quad (63)$$

is the steady state activity of the network, i.e., the average number of transitions per time interval in the steady state. We note that a term related to activity also appears in a fluctuation dissipation relation for nonequilibrium steady states [43].

Due to the Gallavotti-Cohen symmetry (11) the exponential bound can also be written as

$$\lambda(\mathbf{z}) \geq R(e^{(-\mathcal{A}-\mathbf{z}) \cdot \mathbf{J}/R} - 1), \quad (64)$$

where we set  $\eta = R^{-1}$ . This bound is sharper than (61) for  $\mathbf{z} \cdot \mathbf{J} < -\mathcal{A} \cdot \mathbf{J}/2 = \sigma/2$ . Combining Eqs. (61) and (64) we obtain the exponential bound

$$\lambda(\mathbf{z}) \geq R \left[ e^{(|\sigma/2 + \mathbf{z} \cdot \mathbf{J}| - \sigma/2)/R} - 1 \right]. \quad (65)$$

For an individual current  $X_\alpha$ , the exponential bound reads

$$\lambda_\alpha(\mathbf{z}) \geq R \left[ e^{(|\sigma/2 + z J_\alpha| - \sigma/2)/R} - 1 \right]. \quad (66)$$

The choice  $\mathbf{z} = z \mathcal{A}$  in Eq. (65) leads to

$$\lambda_s(z) \geq R \left[ e^{(|\sigma/2 + z \sigma| - \sigma/2)/R} - 1 \right] \quad (67)$$

for the entropy change.

An illustration of the exponential bound (65) is provided in Fig. 8. This bound is typically tighter than the parabolic bound for far from equilibrium conditions, i.e., for large affinity. For example, for a random walk on a unicyclic network with  $N$  sites, a uniform forward stepping rate  $k$  and a vanishing backward stepping rate, which implies divergent affinity, the bound in Eq. (65) is saturated. Specifically, in this case the generating function is

$$\lambda(z) = k \left( e^{z/N} - 1 \right), \quad (68)$$

the activity is  $R = k$  and the cycle current  $J = k/N$ . For vanishing current at equilibrium, the exponential bound reduces to the trivial statement  $\lambda(z) \geq 0$ .

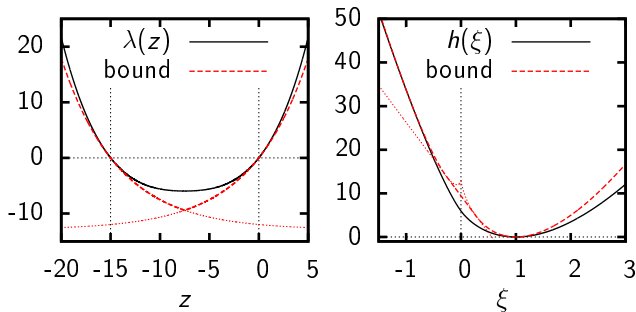


FIG. 8. Generating function (left) and rate function (right) for a five-state unicyclic network with rates  $\ln k_i^+ = (3, 3, 2, 3, 2)$  and  $\ln k_i^- = (-1, 0, -1, 0, 0)$ , affinity  $\mathcal{A} = 15$ , current  $J \simeq 2.25$ , and activity  $R \simeq 12.9$ . The functions are shown as solid lines and the exponential bound (65) as dashed lines. Analytic continuations of the piecewise defined functions are shown as dotted curves.

Our numerics indicates that the hyperbolic cosine bound is always tighter than the exponential bound in unicyclic networks. For multicyclic networks the exponential bound can be tighter. Furthermore, contrary to the hyperbolic cosine bound, the exponential bound does not require knowledge of the topology of the network of states, only the average entropy production and the average activity are required.

In terms of the rate function of an individual current  $X_\alpha$ , corresponding to the generating function Eq. (66), the exponential bound reads

$$h_\alpha(\xi) \leq \begin{cases} \frac{1}{\eta}[1 + \xi - \xi \ln |\xi|] - \sigma\xi, & \xi \leq -e^{-\eta\sigma/2}, \\ \frac{1}{\eta}[1 - \xi + \xi \ln |\xi|], & \xi \geq e^{-\eta\sigma/2}, \\ \frac{1}{\eta}[1 - e^{-\eta\sigma/2}] - \sigma\xi/2, & \text{otherwise.} \end{cases} \quad (69)$$

This bound on the rate function is illustrated in Fig. 8 for a unicyclic network.

Using (22) in the exponential bound (65) for an individual current leads to

$$F_\alpha \geq J_\alpha/R. \quad (70)$$

This new relation provides a lower bound on the dispersion of an individual current, characterized by the Fano factor  $F_\alpha$ , in terms of its average  $J_\alpha$  and the activity  $R$ .

## VII. ASYMPTOTIC BOUNDS

### A. Unicyclic networks

The asymptotic bounds discussed in the following are exact results that become tighter than all previous bounds for large values of  $|z|$ . First we consider a unicyclic network with  $N$  states and affinity  $\mathcal{A}$ . In this case, we can prove the following bound on the generating func-

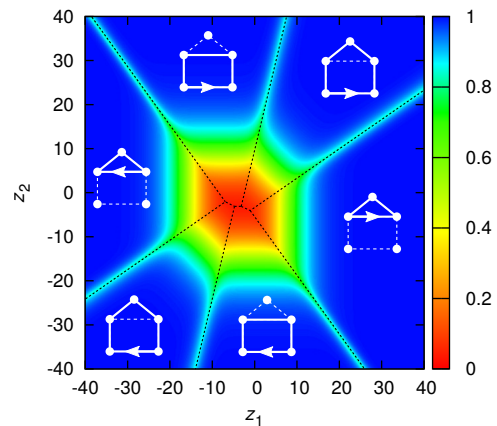


FIG. 9. Asymptotic bound for the house-shaped network with two fundamental cycles shown in Fig. 1b. The color code represents the ratio (77) between the generating function and the bound. Black dashed lines indicate the borders between sectors with constant relevant cycles  $\hat{C}(z)$ . For each sector, the relevant cycle  $\hat{C}(z)$  is shown in white. The affinity of the three-cycle is  $\mathcal{A}_1 = 8$  and the affinity of the four-cycle is  $\mathcal{A}_2 = 6$ .

tion:

$$\lambda(z) \geq J\lambda_{\text{ARW}}(z, \mathcal{A}, N) + r_{\text{ARW}} - \frac{1}{N} \sum_{i=1}^N r_i, \quad (71)$$

where  $\lambda_{\text{ARW}}(z, \mathcal{A}, N)$  is defined in Eq. (37),  $r_{\text{ARW}} \equiv k^+ + k^-$ , and

$$k^\pm \equiv \left( \prod_{i=1}^N k_i^\pm \right)^{1/N}. \quad (72)$$

This bound is proved in appendix D by comparing the weight of a trajectory in the ensemble with transition rates  $k_i^\pm$  with the weight of a trajectory in the ensemble with transition rates  $k^\pm$ . Our numerics indicate that with increasing  $|z|$  the difference between this bound and the actual generating function tends to zero. This fact is quite remarkable given the exponential growth of both functions. Unlike all other bounds presented so far, the bound (47) is not saturated at  $z = 0$ . Only for the case of uniform rates, i.e.,  $k_i^\pm = k^\pm$ , the generating function (36) saturates the bound (71) globally.

### B. Multicyclic networks

In order to obtain an asymptotic bound also valid for multicyclic networks we define an arbitrary closed path  $\mathcal{C}$ , which is a sequence of jumps that finishes at the state it started, as

$$\mathcal{C} \equiv [i(1) \rightarrow i(2) \rightarrow \dots \rightarrow i(n_{\mathcal{C}}) \rightarrow i(1)], \quad (73)$$

where  $n_C$  is the length of the closed path. With this path we associate a geometric mean of the transition rates

$$\gamma_C \equiv (k_{i(1),i(2)} k_{i(2),i(3)} \dots k_{i(n_C),i(1)})^{1/n_C} \quad (74)$$

and integer winding numbers  $m_C^\beta$  that count how often the elementary cycle  $\beta$  is completed within the path  $C$ . Applying a theorem valid for arbitrary non-negative matrices [44, Lemma 3.5.3] to the matrix  $\mathcal{L}_{ij}(z) + \delta_{ij} \max_\ell r_\ell$  we obtain

$$\lambda(z) + \max_\ell r_\ell \geq f(z, C) \equiv \gamma_C \exp\left(\frac{1}{n_C} \sum_\beta m_C^\beta z_\beta\right) \quad (75)$$

for any closed path  $C$ . The best bound on  $\lambda(z)$  in Eq. (75) is obtained by choosing an optimal path  $\hat{C}(z)$ , which in principle depends on  $z$ , that maximizes the r.h.s of Eq. (75) in the large  $z$  regime.

First we consider this optimal path for the unicyclic network. In this case, the optimal path is a single cycle in the forward direction with  $m_C = 1$  if  $z > 0$ . If we consider a path  $C$  with two cycles, i.e.,  $m_C = 2$ , the bound remains the same as the number of states  $n_C$  also doubles. If the closed path is not a direct cycle but contains, for example, one backward jump, then  $\gamma_C$  can become larger. However, such a backward jump also makes  $n_C$  larger and hence, the exponent in Eq. (75) smaller. Since we are interested in the large  $z$  regime, this second effect should be dominant. Hence, for  $z > 0$  the bound (75) leads to

$$\lambda(z) \geq k^+ \exp(z/N) - \max_\ell r_\ell. \quad (76)$$

Even though this bound is different from (71), they both predict the same exponential growth, with the same prefactor, for large  $z > 0$ . The same reasoning is valid for  $z < 0$ , with the optimal path being a single cycle in the negative direction.

For multicyclic networks we consider the house-shaped network with five states shown in Fig. 1b. This network consists of a cycle with three states and affinity  $\mathcal{A}_1$  and a cycle with four states and affinity  $\mathcal{A}_2$ . We choose these cycles to be the fundamental cycles. This network also has a third cycle, which is the cycle with five states and affinity  $\mathcal{A}_1 + \mathcal{A}_2$ . Given a vector  $\mathbf{z} = (z_1, z_2)$ , the optimal path is the cycle that maximizes the r.h.s of Eq. (75). For large enough  $|\mathbf{z}|$ , this optimal path depends only on the direction of the vector. Clearly a path that includes other cycles will lead to a weaker bound.

A contour plot of the ratio  $f(\mathbf{z}, \hat{C}(\mathbf{z})) / [\lambda(\mathbf{z}) + \max_\ell r_\ell]$  for this house-shaped network is shown in Fig. 9. Remarkably, the r.h.s. of (75) captures the leading order of the asymptotics for large  $|\mathbf{z}|$ , i.e., for large  $|\mathbf{z}|$

$$\frac{f(\mathbf{z}, \hat{C}(\mathbf{z}))}{\lambda(\mathbf{z}) + \max_\ell r_\ell} \rightarrow 1. \quad (77)$$

Only in the lines separating regions dominated by different cycles in Fig. 9 does this ratio tend to slightly lower

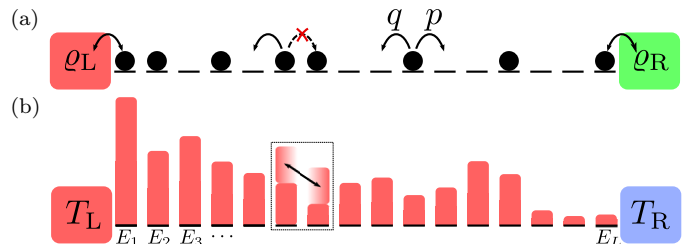


FIG. 10. Schematic illustrations of the WASEP (a) and the KMP (b) models. For the WASEP, in the bulk the particles jump with rates  $p \equiv 1/2 + \nu/(2L)$  to the right and  $q \equiv 1/2 - \nu/(2L)$  to the left, where the SSEP corresponds to  $\nu = 0$ . At the boundaries particles are exchanged with the reservoirs. The model also has the exclusion principle, i.e., the maximum number of particles in a site is one. For the KMP model energy flows from a hot reservoir at temperature  $T_L$  to a cold reservoir at temperature  $T_R$ . In the bulk a randomly chosen pair of sites exchange energy, which is a continuous variable, in such a way that the total energy is conserved. At the boundaries energy is exchanged with the reservoirs. The precise rules of these models can be found in [29] for the WASEP and [28] for the KMP model.

values. Along this line the dominant cycle is degenerate. As shown in appendix E, relation (77) is valid for any multicyclic network. Hence, we conclude that our asymptotic bound predicts the exponential growth of the generating function, apart from exceptional regions in  $\mathbf{z}$  where the optimal cycle is degenerate.

### VIII. PARABOLIC BOUND IN DRIVEN DIFFUSIVE ONE DIMENSIONAL SYSTEMS

We now consider one dimensional driven diffusive systems, which unlike the cases considered so far have a divergent number of states  $L$  in the thermodynamic limit. Calculating the generating function for these systems is a major challenge that can be overcome in some cases with the additivity principle [25]. In this section we compare the parabolic bound to the cumulant generating function obtained from this additivity principle for three examples of driven diffusive systems, for which the validity of the additivity principle has been verified numerically [28, 29].

First we consider the WASEP and the SSEP, which is a particular case of the WASEP. These models are illustrated in Fig. 10 and their precise definition can be found in [26]. In the WASEP particles flow from the left reservoir with constant density  $\rho_L$  to the right reservoir with density  $\rho_R < \rho_L$ . The current of particles in the system is proportional to the entropy production, and the affinity that drives the process out of equilibrium is given by [26, 29]

$$\mathcal{A}_{\text{WASEP}} = -\ln \frac{1 - \rho_L}{\rho_L} + \ln \frac{1 - \rho_R}{\rho_R} + (L - 1) \ln \frac{1 - \nu/L}{1 + \nu/L}. \quad (78)$$

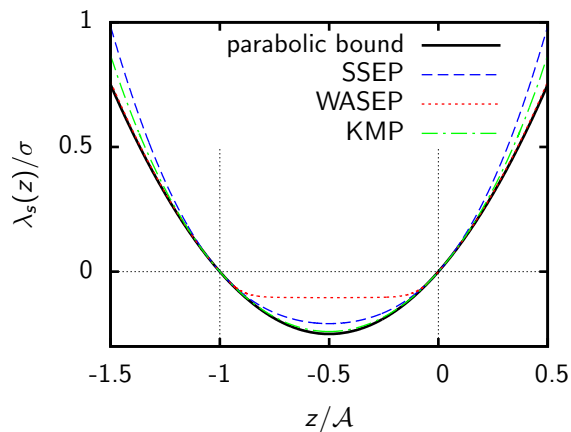


FIG. 11. Comparison of the parabolic bound (42) with generating functions for driven diffusive systems. For the SSEP the densities of the left and right reservoirs were chosen as  $\varrho_L = 0.99$  and  $\varrho_R = 0.01$ . For the WASEP the parameters are  $\nu = 10$ ,  $\varrho_L = 4/7$ , and  $\varrho_R = 5/18$ , as in Ref. [29]. For the KMP model the parameters are  $T_L = 2$  and  $T_R = 1$ , as in Ref. [28].

The weak asymmetry of the bulk rates, which scales with  $1/L$ , guarantees that in the thermodynamic limit  $L \rightarrow \infty$  the affinity is finite. In Fig. 11, we have calculated the generating function using the additivity principle for the SSEP, as explained in [26], and for the WASEP, as explained in [29]. In both cases the generating functions are inside the parabolic bound.

The KMP model is a driven diffusive system for the transport of energy from a reservoir at temperature  $T_L$  to a reservoir at temperature  $T_R < T_L$ , as illustrated in Fig. 10. A key feature of the KMP model is that there is no dissipation in the bulk. The precise definition of the model can be found in [28]. The heat transfer from the left to the right reservoir is proportional to the entropy production with the affinity given by [28]

$$\mathcal{A}_{\text{KMP}} = (T_R^{-1} - T_L^{-1}). \quad (79)$$

The generating function for this model, which is obtained from the additivity principle as explained in [28], also satisfies the parabolic bound in Fig. 11 within the finite support  $-T_R^{-1} < z < T_L^{-1}$  of  $\lambda(z)$ . As a consequence, the rate function satisfies the corresponding parabolic bound globally.

These results demonstrate that our parabolic bound is even more universal: it seems to be valid for these driven diffusive systems in the thermodynamic limit, for which the number of states diverges. We expect that the parabolic bound is the only relevant one in the limit  $L \rightarrow \infty$ . The hyperbolic cosine bound (57) approaches the parabolic bound for vanishing affinity per number of states in a cycle. The exponential bound (61) degenerates with increasing activity to a linear function, which reflects simply the convexity of the generating function.

Another interesting issue will be to explore whether the bound is still valid in the  $L \rightarrow \infty$  limit if the sys-

tem undergoes a dynamical phase transition as the KMP model in a ring-like geometry [45].

## IX. CONCLUSIONS

We have obtained four global bounds on current fluctuations for Markov processes in steady states summarized in table I. The parabolic bound from Sec. IV is the most universal result of this paper. The simple knowledge of the average entropy production is enough to bound the whole range of fluctuations of any individual current. In other words, for nonequilibrium steady states, the generating function associated with any fluctuating current must lie inside the parabola shown in Fig. 12. The universality of the parabolic bound was further confirmed by the fact that it also applies to the three driven diffusive systems we analyzed in Sec. VIII, for which the number of states diverges.

This parabolic bound can be saturated only close to equilibrium. A bound that is generally tighter than the parabolic bound, particularly if the system is far from equilibrium, is the hyperbolic cosine bound from Sec. V. This necessarily less universal bound also requires knowledge of the thermodynamic forces, i.e., the affinities, that drive the process out of equilibrium and of the topology of the network of states.

The exponential bound depends on the average entropy production and on the average number of transitions per time. In contrast to the parabolic and hyperbolic cosine bounds that are conjectures based on extensive numerical evidence, we have proven the exponential bound. It is typically tighter than the parabolic bound for far from equilibrium situations. While for a unicyclic network we observed that the hyperbolic cosine bound is always tighter than the exponential bound, for multicyclic networks the exponential bound can be tighter.

The fourth bound is an exact asymptotic bound that predicts the growth of the generating function for large  $z$ , as illustrated in Fig. 12. This bound requires knowledge of the particular transition rates. Therefore, its importance arises in a situation where a Markov process with all its transition rates is given but calculating the full generating function is not possible.

Summarizing, typical and large fluctuations for any individual current in stationary Markov processes, which are used to describe a large amount of nonequilibrium systems ranging from enzymatic reactions to nanoscale electronic systems, have been shown to be bounded by the average entropy production or the average entropy production and the average activity. Rigorous proofs of the parabolic bound and of the hyperbolic cosine bound remain as main open technical challenges.

*Note added:* A proof of the parabolic bound has recently appeared [46].

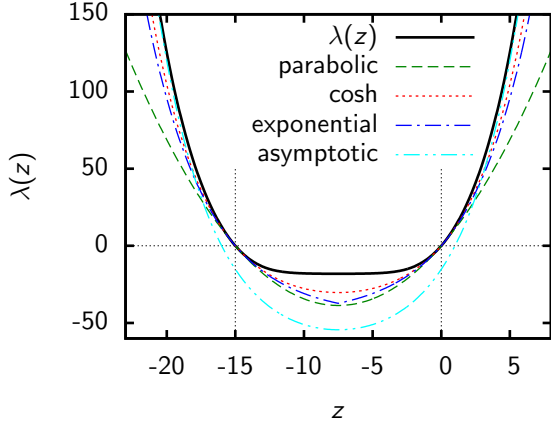


FIG. 12. Summary of the four bounds for a unicyclic network with four states. Transition rates are  $\ln k_i^+ = (3, 4, 5, 4)$  and  $\ln k_i^- = (0, -1, 1, 1)$ , leading to the affinity  $\mathcal{A} = 15$  and the current  $J \simeq 10.307$ .

<b>Parabolic</b>	$z \cdot \mathbf{J} (1 + z \cdot \mathbf{J} / \sigma)$	(31)
------------------	--	------

<b>Hyperbolic cosine</b>	$\sigma \frac{\cosh \left[ \left( \frac{z \cdot \mathbf{J}}{\sigma} + \frac{1}{2} \right) \frac{\mathcal{A}^*}{n^*} \right] - \cosh \left[ \mathcal{A}^* / (2n^*) \right]}{(\mathcal{A}^* / n^*) \sinh \left[ \mathcal{A}^* / (2n^*) \right]}$	(58)
--------------------------	--	------

<b>Exponential</b>	$R \left[ e^{( \sigma/2 + z \cdot \mathbf{J}  - \sigma/2)/R} - 1 \right]$	(65)
--------------------	---	------

<b>Asymptotic</b>	$-\max_{\ell} r_{\ell} + \gamma_C \exp \left( \frac{1}{n_C} \sum_{\beta} m_C^{\beta} z_{\beta} \right)$	(75)
-------------------	---	------

TABLE I. Summary of lower bounds on the generating function.

### Appendix A: Proof of the exponential bound

The theorem by Ellis [20, Theorem IX.4.4] can be stated as follows. For any non-negative matrix  $B_{ij}$ , the associated maximum eigenvalue can be calculated as

$$\ln \mu = \sup_{\tau_{ij}} \sum_{i,j} \tau_{ij} \ln \frac{B_{ij} \nu_i}{\tau_{ij}}, \quad (\text{A1})$$

where  $\nu_i \equiv \sum_k \tau_{ik}$  and  $0 \ln 0 \equiv 0$ . The admissible matrices  $\tau_{ij}$  must satisfy the following properties:

1. Normalization,

$$\sum_{i,j} \tau_{ij} = \sum_i \nu_i = 1. \quad (\text{A2})$$

2. Equal row- and column-sums,

$$\nu_i \equiv \sum_{\ell} \tau_{i\ell} = \sum_{\ell} \tau_{\ell i}. \quad (\text{A3})$$

3. Non-negative with the same (or less complex) structure as  $B_{ij}$ , i.e.,

$$\tau_{ij} > 0 \Rightarrow B_{ij} > 0. \quad (\text{A4})$$

In order to apply Eq. (A1) to the modified Markov generator  $\mathcal{L}_{ij}(\mathbf{z})$ , we consider the matrix

$$B_{ij}(\mathbf{z}) \equiv \delta_{ij} + \eta \mathcal{L}_{ij}(\mathbf{z}), \quad (\text{A5})$$

with a sufficiently small parameter  $\eta > 0$ . Its largest eigenvalue is  $1 + \eta \lambda(\mathbf{z})$ . Lower bounds on the generating function  $\lambda(\mathbf{z})$  can be obtained from (A1) by choosing an appropriate matrix  $\tau_{ij}$ . The choice

$$\tau_{ij} = B_{ij}(0) p_j^s \quad (\text{A6})$$

saturates the bound for  $\mathbf{z} = 0$ . The bound for the eigenvalue (A1) then reads (with  $\nu_i = p_i^s$ )

$$\ln[1 + \eta \lambda(\mathbf{z})] \geq \sum_{i,j} [\delta_{ij} + \eta \mathcal{L}_{ij}(0)] p_j^s \ln \frac{[\delta_{ij} + \eta \mathcal{L}_{ij}(\mathbf{z})] p_i^s}{[\delta_{ij} + \eta \mathcal{L}_{ij}(0)] p_j^s}. \quad (\text{A7})$$

Since  $\mathcal{L}_{ii}(\mathbf{z}) = \mathcal{L}_{ii}(0)$  the logarithm vanishes for  $i = j$  and the r.h.s. simplifies to

$$\begin{aligned} \ln[1 + \eta \lambda(\mathbf{z})] &\geq \sum_{i \neq j} \eta \mathcal{L}_{ij}(0) p_j^s \ln \frac{\mathcal{L}_{ij}(\mathbf{z}) p_i^s}{\mathcal{L}_{ij}(0) p_j^s} \quad (\text{A8}) \\ &= \eta \sum_{i \neq j} p_j^s k_{ji} \left( z \cdot \mathbf{d}_{ji} + \ln \frac{p_i^s}{p_j^s} \right). \quad (\text{A9}) \end{aligned}$$

The term proportional to  $\ln(p_i^s/p_j^s)$  vanishes because  $p_i^s$  is the stationary distribution. Identifying the stationary current  $\mathbf{J} = \sum_{i \neq j} p_i^s k_{ij} \mathbf{d}_{ij}$  we obtain the bound

$$\lambda(\mathbf{z}) \geq \frac{1}{\eta} (e^{\eta \mathbf{z} \cdot \mathbf{J}} - 1), \quad (\text{A10})$$

which is Eq. (61) in the main text.

The bound improves for larger  $\eta$ . The maximal value that still complies with the requirement for positive entries  $B_{ij}$  is the inverse of the maximal escape rate  $\eta = 1/\max_i(r_i)$ . In this case, the proof of (A1) in Ref. [20] uses the equation

$$\sum_{i,j} \tau_{ij} \ln \frac{B_{ij} \nu_i}{\tau_{ij}} = \sum_{i,j} \tau_{ij} \ln \frac{B_{ij} \nu_i^0}{\tau_{ij}^0} - \sum_{i,j} \tau_{ij} \ln \frac{\tau_{ij} \nu_i^0}{\nu_i \tau_{ij}^0}, \quad (\text{A11})$$

where  $\nu_i^0 = \sum_j \tau_{ij}^0$ . The matrix  $\tau^0$  is given by

$$\tau_{ij}^0 = \tilde{q}_i B_{ij} q_j / \mu, \quad (\text{A12})$$

where  $\tilde{q}$  and  $q$  are left and right eigenvectors of  $B$ , respectively, with the normalization  $\sum_i q_i = 1$  and  $\sum_i \tilde{q}_i q_i = 1$ . From relations (A2), (A3), and (A12) it follows that the first sum in Eq. (A11) is simply  $\ln \mu$ . The second sum with a minus sign can be shown to fulfill the inequality

$$\sum_{i,j} y_{ij} x_{ij} \ln x_{ij} \geq \sum_{i,j} y_{ij} (x_{ij} - 1) = \sum_{i,j} (\tau_{ij} - y_{ij}) = 0, \quad (\text{A13})$$

where

$$y_{ij} \equiv \frac{\nu_i \tau_{ij}^0}{\nu_i^0}, \quad x_{ij} \equiv \frac{\tau_{ij} \nu_i^0}{\nu_i \tau_{ij}^0}. \quad (\text{A14})$$

Equality in Eq. (A13) is achieved for  $\tau_{ij} = \tau_{ij}^0$ , which with Eq. (A13) provides a proof of (A1).

Actually, we can show that the bound (A10) is valid even for larger values of  $\eta$  up to  $\eta = R^{-1}$ , where  $R$  is the average activity in Eq. (63). In this case, the diagonal elements  $B_{ii}$  can be negative. This property can affect Eq. (A13), which requires that  $x_{ij} \geq 0$  and  $y_{ij} \geq 0$ . For  $B_{ij}(z) = \delta_{ij} + \eta \mathcal{L}_{ij}^\alpha(z)$ , if

$$1 + \eta \lambda_\alpha(z) > 0 \quad (\text{A15})$$

then all  $x_{ij}$  and  $y_{ij}$  in Eq. (A14) for  $i \neq j$  are non-negative. The inequality (A13) is then valid for  $i \neq j$  with condition (A15). For the diagonal terms we can write

$$\begin{aligned} \sum_i y_{ii} x_{ii} \ln x_{ii} &= \sum_i p_i^s (1 - \eta r_i) \ln[1 + \eta \lambda_\alpha(z)] \\ &\geq \sum_i p_i^s (1 - \eta r_i) \frac{\eta \lambda_\alpha(z)}{1 + \eta \lambda_\alpha(z)}, \end{aligned} \quad (\text{A16})$$

where the inequality is valid for  $\eta \leq R^{-1}$  and if condition (A15) is fulfilled. Therefore, if condition (A15) holds then the inequality (A14) is valid for  $\eta \leq 1/R$ .

Since this condition (A15) is valid for  $z = 0$ , it must also be valid for some finite range in  $z$ . Using a simple self-consistency check, we can even prove that this ‘‘finite range’’ must in fact always be infinite. Assume the function  $1 + \lambda_\alpha(z)/R$  crosses zero at some value  $z = z^*$ . Then the condition (A15) is violated for  $z = z^* - \delta z$ . On the other side, for  $z = z^* + \delta z$ , the condition is still satisfied and we find

$$1 + \lambda_\alpha(z^* + \delta z)/R \geq e^{(z^* + \delta z)J_\alpha/R} > 0, \quad (\text{A17})$$

which contradicts the continuity of  $\lambda_\alpha(z)$ .

## Appendix B: Numerical verification

The numerical verification of the conjectured bounds was performed on large sets of networks with different transition rates. The corresponding generating functions are given by the largest eigenvalues of the matrices  $\mathcal{L}(z)$ . We calculated these eigenvalues using standard numerical algorithms. The stationary distributions  $p_i^s$ , which are computed as the eigenvector for  $z = 0$ , are used to evaluate the steady state currents that appear in the bounds. The precise procedures are described below.

## 1. Unicyclic networks

For unicyclic networks with  $N$  states it is convenient to parametrize the transition rates (47) as

$$k_i^\pm = \exp(\phi_i \pm \theta_i \mathcal{A}/2). \quad (\text{B1})$$

The global time scale can be fixed by requiring  $\sum_i \phi_i = 0$ . Thus we avoid numerical instabilities due to extremely large or small matrix entries. Moreover, in order to sample cycles with predefined affinity  $\mathcal{A}$ , we require  $\sum_i \theta_i = 1$ . We generate vectors  $\phi'_i$  and  $\theta'_i$  of  $N$  independent and identically distributed random numbers. The above constraints are satisfied by setting  $\phi_i = \phi'_i - \bar{\phi}'$  and  $\theta_i = \theta'_i / \bar{\theta}'$ , where the overbar denotes the average of the vectors elements within the realization. Samples where at least one of the  $|\theta_i|$  is above a certain value were discarded in order to avoid numerical instabilities. The cut-off value 1 turns out to be suitable for this purpose. Since the transition rates associated with the discarded samples are extremely non-uniform, the corresponding generating function lies close to the (proven) upper bound anyway.

For the plots shown in Fig. 6,  $\phi'_i$  and  $\theta'_i$  were drawn from uniform distributions with  $0 < \phi'_i < 4$  and  $-0.5 < \theta'_i < 0.5$ , respectively. The generating functions were calculated for a total of 10 000 samples for each affinity, of which only the first 100 are shown in the figure. For cycles with many states and high affinity, it is virtually impossible to cover the whole area between the upper and the lower bound using a single, simple distribution for  $\phi'_i$  and  $\theta'_i$ . In Fig. 5, we show several families of sample generating functions where the rates are drawn from different statistical ensembles. Specifically,  $\phi'_i$  and  $\theta'_i$  are both Gaussian random variables with mean 1 (which is irrelevant for  $\phi_i$ ) and standard deviations (SD) reaching from 0.01 to 2.

In principle the lengths sub-steps  $d_{i,i+i}$  can be distributed arbitrarily among the edges of the network. In most cases, the choice  $d_{i,i+i} \propto \ln(k_i^+/k_i^-)$  avoids numerical instabilities. In order to pre-assess the range of  $z$  we can make use of the proven asymptotic bound (71): the validity of the hyperbolic cosine bound has to be checked only in the finite range where it is weaker than the asymptotic bound. In all cases the hyperbolic cosine bound (50) is satisfied. Since the hyperbolic cosine bound implies the parabolic bound, this numerical evidence also allows us to conjecture the parabolic bound for unicyclic networks.

## 2. Multicyclic networks

The bounds relevant for a numerical test for multicyclic networks are the parabolic bound and the hyperbolic cosine bound. They exist in the formulation for entropy change [Eqs. (44) and (55)] and for arbitrary individual currents [Eqs. (43) and (57)]. The former type can be

checked by setting the matrix of increments in Eq. (7) to  $d_{ij}^s = \ln(k_{ij}/k_{ji})$ , for the latter we use anti-symmetrized Gaussian random matrices for  $d_{ij}^c$ .

We have performed two types of tests. The first type relies on random rate matrices  $k_{ij}$  of dimension  $N \times N$ , each of them corresponding to a fully connected network with  $N$  states. The rates were generated according to

$$k_{ij} = \exp[a(\phi_{ij} + \phi_{ji})/2 + b\theta_{ij}], \quad (\text{B2})$$

where  $\phi_{ij}$  and  $\theta_{ij}$  are independent Gaussian random numbers with zero mean and variance 1. The parameters  $a$  and  $b$  can be used to tune the properties of the network. While small values of  $a$  simulate fully connected networks, larger values of  $a$  typically suppress some of the transitions, so that the generated matrices effectively correspond to partially connected networks with random topology. The parameter  $b$  introduces an asymmetry in the transitions, that drives the system out of equilibrium. For smaller values of  $b$  the generating functions lie closer to the parabolic bound. For Fig. 4 we have calculated 300 generating functions for each  $N = 4$  and  $N = 6$  with  $a = 5$  and  $b = 2$ . In a more extensive computation, we have checked the parabolic bound for a total of  $10^7$  generating functions with  $a$  ranging from 0 to 5,  $b$  ranging from 0.01 to 5, and  $N$  ranging from 4 to 50. The hyperbolic cosine bound could be checked only up to  $N = 8$ , for larger networks the determination of the relevant cycle in (57) becomes numerically expensive.

The second type of test applies to small networks with given topology, where the fundamental cycles can be identified by hand. The affinities of these cycles can be fixed, so that the bounds (55) and (57) depend only on the steady state currents. For example, for the network shown in Fig. 1c, random rates were assigned to most of the transition. The random numbers were generated such that  $\ln k_{ij}$  were Gaussian random numbers with standard deviations ranging from 0.01 to 3 and, at first, with zero mean. Only the three forward transition rates in the cycle (1,2,3,1) were determined algebraically from the other transition rates and the constraints from the fixed cycle affinities  $\mathcal{A}_1$ ,  $\mathcal{A}_2$  and  $\mathcal{A}_3$ . Typically, the generating functions obtained via this procedure are quite far from the hyperbolic cosine bound. In order to test also more critical cases, we have added a bias  $\pm \mathcal{A}^*/(2n^*)$  to the logarithms of the forward (+) and backward (-) transition rates constituting the relevant cycle for the hyperbolic cosine bound. Moreover, the rates for transitions exiting the relevant cycle were gradually lowered by several orders of magnitude. For the plots in Fig. 7, we have used attenuations of these rates between  $e^0$  and  $e^{-25}$ . Similar tests were performed for a large varieties of networks (as the networks shown in Fig. 2 of the supplementary material of Ref. [17]).

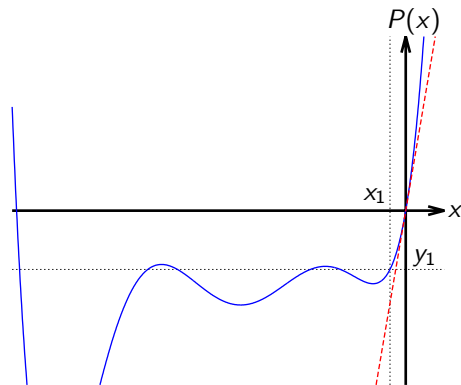


FIG. 13. The polynomial  $P(x)$  for a generic unicyclic network with  $N = 6$  states. The tangent at  $x = 0$  and the values  $y = y_1$  and  $x = x_1$  are shown as dashed lines.

### Appendix C: Proof of the upper bound on the generating function for unicyclic networks

For unicyclic networks with  $N$  states the tilted Markov generator has the tridiagonal shape

$$\mathcal{L}(z) = \begin{pmatrix} -r_1 & \tilde{k}_{21} & 0 & 0 & \dots & \tilde{k}_{N1} \\ \tilde{k}_{12} & -r_2 & \tilde{k}_{32} & 0 & \dots & 0 \\ 0 & \tilde{k}_{23} & -r_3 & \tilde{k}_{43} & \ddots & 0 \\ 0 & 0 & \tilde{k}_{34} & -r_4 & \ddots & \vdots \\ \vdots & \vdots & \ddots & \ddots & \ddots & \tilde{k}_{N,N-1} \\ \tilde{k}_{1N} & 0 & 0 & \dots & \tilde{k}_{N-1,N} & -r_N \end{pmatrix} \quad (\text{C1})$$

with  $\tilde{k}_{ij} \equiv k_{ij}e^{zd_{ij}}$ . The displacements  $d_{ij}$  must satisfy  $d_{ij} = -d_{ji}$ . If the observable of interest is the number of turnovers, the displacements must add up to the cycle affinity  $d_{12} + d_{23} + \dots + d_{N1} = 1$ . It should be kept in mind that any statistical quantity in the long time limit (in particular the generating function and the rate function) do not depend on the specific choice of the individual  $d_{ij}$ .

The characteristic polynomial associated with the matrix (C1) reads

$$\begin{aligned} \chi(z, x) &\equiv \det(\mathcal{L}(z) - x\mathbf{1}_N) \\ &= \sum_{\pi} (-1)^{\pi} \prod_{i=1}^N (\mathcal{L}_{i\pi(i)}(z) - x\delta_{i\pi(i)}), \end{aligned} \quad (\text{C2})$$

where the sum runs over all permutations  $\pi$  of the indices  $i = 1, \dots, N$  and  $\mathbf{1}_N$  is the  $N \times N$  identity matrix. We identify  $0 \equiv N$  and  $N + 1 \equiv 1$  for the indices of matrix entries. There are two types of terms in (C2) that contain a specific rate  $\tilde{k}_{i+1,i}$ : the contribution from the next row  $i + 1$  can either be  $\tilde{k}_{i,i+1}$  or  $\tilde{k}_{i+2,i+1}$ . For the former type the  $z$ -dependence cancels out due to  $d_{i+1,i} = -d_{i,i+1}$  and we end up with the constant factor  $\tilde{k}_{i+1,i}\tilde{k}_{i,i+1} = k_{i+1,i}k_{i,i+1}$ . Terms of the latter type must also contain  $\tilde{k}_{i,i-1}$  as the only possible contribution from the previous

column  $i - 1$ . Iteratively, we see that there can be only one term of this type, namely the one that contains all forward transitions

$$\tilde{k}_{12}\tilde{k}_{23}\dots\tilde{k}_{N1} = k_{12}k_{23}\dots k_{N1}e^z \equiv \Gamma^+e^z. \quad (\text{C3})$$

An analogous argument can be set up for the lower off-diagonal of the matrix with the  $z$ -dependent term

$$\begin{aligned} \tilde{k}_{21}\tilde{k}_{32}\dots\tilde{k}_{1N} &= k_{21}k_{32}\dots k_{1N}e^{-z} \\ &\equiv \Gamma^-e^{-z} = \Gamma^+e^{-(z+\mathcal{A})}. \end{aligned} \quad (\text{C4})$$

All other terms in the determinant (C2) do not depend on  $z$  and we can write

$$\chi(z, x) = (-1)^{N+1}[\Gamma^+e^z + \Gamma^-e^{-z} - (\Gamma^+ + \Gamma^-) - P(x)] \quad (\text{C5})$$

with some polynomial  $P(x)$  that is independent of  $z$  and the specific choice of the  $d_{ij}$ . The alternating prefactor is due to the fact that the permutations associated with the terms (C3) and (C4) are either odd or even, depending on the number of states  $N$ . The generating function is thus given by

$$\begin{aligned} \lambda(z) &= P^{-1}(\Gamma^+e^z + \Gamma^-e^{-z} - \Gamma^+ - \Gamma^-) \\ &= P^{-1}\left(2\sqrt{\Gamma^+\Gamma^-}[\cosh(z + \mathcal{A}/2) - \cosh(\mathcal{A}/2)]\right), \end{aligned} \quad (\text{C6})$$

where the function  $P^{-1}(y)$  returns the root of the polynomial  $P(x) - y$  that has the largest real part. Due to the Perron-Frobenius theorem, this root must be real for all arguments occurring in (C6), i.e., for all  $y \geq y_1 \equiv 2\sqrt{\Gamma^+\Gamma^-}[1 - \cosh(\mathcal{A}/2)]$ . The root associated with the minimal argument  $y_1$  is  $x_1 \equiv P^{-1}(y_1) = \min_z \lambda(z) =$

$\lambda(-\mathcal{A}/2)$ . Obviously, the polynomial  $P(x)$  (see Fig. 13) has the properties  $P(0) = \chi(0, 0) = 0$  and

$$\begin{aligned} \lim_{x \rightarrow \infty} P(x) &= (-1)^N \lim_{x \rightarrow \infty} \chi(z, x) \\ &= \lim_{x \rightarrow \infty} (-1)^N \det(-x\mathbf{1}_N) = +\infty. \end{aligned} \quad (\text{C7})$$

Since the matrix  $\mathcal{L}(-\mathcal{A}/2)$  can be brought to a symmetric form by choosing  $d_{ij} = \ln(k_{ij}/k_{ji})/\mathcal{A}$ , the corresponding characteristic polynomial  $P(x) - y_1$  has only real roots  $x_i$  with  $x_1$  denoting the largest one. The second derivative of  $P(x)$  is

$$P''(x) = \frac{d^2}{dx^2} \left[ y_1 + \prod_{i=1}^N (x - x_i) \right] = \sum_{i=1}^N \sum_{j=1}^N \prod_{\substack{\ell=1 \\ j \neq i \\ i \neq \ell \neq j}}^N (x - x_\ell). \quad (\text{C8})$$

For  $x > x_1$  this expression is positive so that  $P(x)$  is convex. As a consequence, the inverted function  $P^{-1}(y)$  is concave for the relevant arguments  $y > y_1$ . Hence it satisfies

$$P^{-1}(y) \leq (P^{-1})'(0) y \quad (\text{C9})$$

with equality for  $y = 0$ . This relation leads to the upper bound

$$\lambda(z) \leq 2\sqrt{\Gamma^+\Gamma^-}(P^{-1})'(0) [\cosh(z + \mathcal{A}/2) - \cosh(\mathcal{A}/2)] \quad (\text{C10})$$

holding with equality for  $z = 0$ . The prefactor in this bound is equal to the one in Eq. (51), as can be seen by calculating steady state current from Eq. (C6),

$$J = \lambda'(z) = 2\sqrt{\Gamma^+\Gamma^-}(P^{-1})'(0) \sinh(\mathcal{A}/2). \quad (\text{C11})$$

#### Appendix D: Proof of the asymptotic bound for unicyclic networks

First we restrict to a unicyclic network with  $N$  states, affinity  $\mathcal{A}$  and transition rates

$$k_{ij} \equiv \delta_{i,i+1}k_i^+ + \delta_{i+1,i}k_{i+1}^-. \quad (\text{D1})$$

A stochastic path  $n(\tau)$  is defined by the sequence of jumps  $n_\ell \rightarrow n_{\ell+1}$  between adjacent states that occur at times  $\tau_\ell$ . The weight of this path is given by

$$\mathcal{P}[n(\tau)] = \prod_{\ell} k_{n_\ell n_{\ell+1}} \exp[-r_{n_\ell}(\tau_{\ell+1} - \tau_\ell)], \quad (\text{D2})$$

where the sum runs over all jumps. The weight of a path with modified transition rates  $\tilde{k}_{ij}$  reads

$$\tilde{\mathcal{P}}[n(\tau)] = \prod_{\ell} \tilde{k}_{n_\ell n_{\ell+1}} \exp[-\tilde{r}_{n_\ell}(\tau_{\ell+1} - \tau_\ell)]. \quad (\text{D3})$$

For these modified transition rates we choose an asymmetric random walk, i.e.,

$$\tilde{k}_{ij} \equiv \delta_{i,i+1}k^+ + \delta_{i+1,i}k^- \quad (\text{D4})$$



with

$$k^\pm \equiv \left( \prod_{i=1}^N k_i^\pm \right)^{1/N}, \quad (\text{D5})$$

which leads to  $\tilde{r} \equiv k^+ + k^-$ . Ensemble averages using the path weight  $\tilde{\mathcal{P}}[n(\tau)]$  are denoted as  $\langle \dots \rangle_{\text{ARW}}$ . The generating function can be rewritten as

$$\begin{aligned} \lambda(z) &= \frac{1}{t} \ln \left\langle e^{zX[n(\tau)]} \right\rangle = \frac{1}{t} \ln \int \mathcal{D}_{n(\tau)} e^{zX[n(\tau)]} \frac{\mathcal{P}[n(\tau)]}{\tilde{\mathcal{P}}[n(\tau)]} \tilde{p}[n(\tau)] \\ &= \frac{1}{t} \ln \left\langle e^{zX[n(\tau)]} \prod_{i=1}^N \left( \frac{k_i^+}{\gamma^+} \right)^{m_i^+} \left( \frac{k_i^-}{\gamma^-} \right)^{m_i^-} e^{-(r_i - \tilde{r}_i) \mathcal{T}_i} \right\rangle_{\text{ARW}}, \end{aligned} \quad (\text{D6})$$

where the integration in the first line is over all stochastic trajectories. The path dependent variables  $m_i^\pm$  count the jumps out of state  $i$  in forward or backward direction and  $\mathcal{T}_i$  is the total sojourn time in state  $i$ . These variables are identically distributed in the ARW-ensemble.

The probability  $\tilde{P}(X)$  is the probability that the fluctuating current is  $X$  in the ARW-ensemble. It is the sum of the weight of all trajectories for which the current is  $X$ . Using this  $\tilde{P}(X)$  Eq. (D6) can be written as

$$\begin{aligned} \lambda(z) &= \frac{1}{t} \ln \sum_X \tilde{p}(X) e^{zX} \left\langle \exp \left[ \sum_{i=1}^N m_i^+ \ln(k_i^+ / \gamma^+) + \sum_{i=1}^N m_i^- \ln(k_i^- / \gamma^-) - \sum_{i=1}^N (r_i - \tilde{r}) \mathcal{T}_i \right] \middle| X \right\rangle_{\text{ARW}} \\ &\geq \frac{1}{t} \ln \sum_X \tilde{p}(X) e^{zX} \exp \left[ \sum_{i=1}^N \langle m_i^+ | X \rangle_{\text{ARW}} \ln(k_i^+ / \gamma^+) + \sum_{i=1}^N \langle m_i^- | X \rangle_{\text{ARW}} \ln(k_i^- / \gamma^-) - \sum_{i=1}^N (r_i - \tilde{r}) t / N \right], \end{aligned} \quad (\text{D7})$$

where the conditioned average in the first line represents a functional integration over all trajectories with fluctuating current equal to  $X$  and we used Jensen's inequality from the first to the second line. Due to (D5) the terms with the logarithms vanish, leading to the final result in Eq. (71).

### Appendix E: Proof of the asymptotic limit (77) for multicyclic networks

For general Markov generators  $\mathcal{L}(z)$ , as defined in Eq. (7), the determinant (C2) can be written as

$$0 = \chi(z, \lambda(z)) = \prod_{i=1}^N [-r_i - \lambda(z)] + \sum_{\mathcal{C}} (-1)^{\mathcal{C}} \gamma_{\mathcal{C}}^{n_{\mathcal{C}}} e^{\mathbf{m}_{\mathcal{C}} \cdot \mathbf{z}} \prod_{j \notin \mathcal{C}} [-r_j - \lambda(z)], \quad (\text{E1})$$

where the sum runs over all combinations of disjoint cycles in the underlying network and  $(-1)^{\mathcal{C}}$  denotes the sign of the corresponding permutations in the determinant. For each  $\mathcal{C}$ , the quantities  $n_{\mathcal{C}}$ ,  $\gamma_{\mathcal{C}}$  and  $\mathbf{m}_{\mathcal{C}}$  are defined as for the individual cycles in Sec. VII of the main text. Dividing Eq. (E1) by  $\lambda(z)^N$  leads to

$$0 = \prod_{i=1}^N [-r_i / \lambda(z) - 1] + \sum_{\mathcal{C}} (-1)^{\mathcal{C}} f(z, \mathcal{C})^{n_{\mathcal{C}}} \lambda(z)^{-n_{\mathcal{C}}} \prod_{j \notin \mathcal{C}} [-r_j / \lambda(z) - 1], \quad (\text{E2})$$

where  $f(z, \mathcal{C})$  is defined in Eq. (75). We now analyze the limit  $|z| \rightarrow \infty$  with the direction  $\mathbf{z}/|z|$  kept fixed. Making use of the (already proven) lower bound (75) with the optimal path  $\hat{\mathcal{C}} \equiv \hat{\mathcal{C}}(z)$ , we see that  $r_i / \lambda(z)$  and the terms with  $(\mathbf{m}_{\mathcal{C}} \cdot \mathbf{z}) / n_{\mathcal{C}} < \mathbf{m}_{\hat{\mathcal{C}}} \cdot \mathbf{z} / n_{\hat{\mathcal{C}}}$  vanish in this limit. Provided that the optimal cycle is unique, we are left with

$$0 = (-1)^N + \lim_{|z| \rightarrow \infty} (-1)^{1+n_{\hat{\mathcal{C}}}} f(z, \hat{\mathcal{C}})^{n_{\hat{\mathcal{C}}}} \lambda(z)^{-n_{\hat{\mathcal{C}}}} (-1)^{N-n_{\hat{\mathcal{C}}}}, \quad (\text{E3})$$

which leads to

$$\lim_{|z| \rightarrow \infty} \frac{f(z, \hat{\mathcal{C}})}{\lambda(z)} = 1. \quad (\text{E4})$$

In Eq. (77), the constant  $\max_{\ell} r_{\ell}$  is added to the denominator without harm, in order to make the ratio positive everywhere. The essential ingredient in this proof is the uniqueness of the optimal cycle  $\hat{C}$ . Only in peculiar regions the vector  $\mathbf{z}$  leads to more than one cycle with the same value of  $\mathbf{m}_{\hat{C}} \cdot \mathbf{z}/n_{\hat{C}}$ . For example, these regions show up in Fig. 9 as the lines along which the ratio (77) differs from 1.

- 
- [1] D. J. Evans, E. G. D. Cohen, and G. P. Morriss, “Probability of second law violations in shearing steady states,” *Phys. Rev. Lett.* **71**, 2401 (1993).
- [2] D. J. Evans and D. J. Searles, “Equilibrium microstates which generate second law violating steady states,” *Phys. Rev. E* **50**, 1645 (1994).
- [3] G. Gallavotti and E. G. D. Cohen, “Dynamical ensembles in nonequilibrium statistical mechanics,” *Phys. Rev. Lett.* **74**, 2694 (1995).
- [4] J. Kurchan, “Fluctuation theorem for stochastic dynamics,” *J. Phys. A: Math. Gen.* **31**, 3719 (1998).
- [5] J. L. Lebowitz and H. Spohn, “A Gallavotti-Cohen-type symmetry in the large deviation functional for stochastic dynamics,” *J. Stat. Phys.* **95**, 333 (1999).
- [6] U. Seifert, “Stochastic thermodynamics, fluctuation theorems, and molecular machines,” *Rep. Prog. Phys.* **75**, 126001 (2012).
- [7] T. Speck, V. Blickle, C. Bechinger, and U. Seifert, “Distribution of entropy production for a colloidal particle in a nonequilibrium steady state,” *EPL* **79**, 30002 (2007).
- [8] J. Mehl, B. Lander, C. Bechinger, V. Blickle, and U. Seifert, “Role of hidden slow degrees of freedom in the fluctuation theorem,” *Phys. Rev. Lett.* **108**, 220601 (2012).
- [9] J. R. Gomez-Solano, A. Petrosyan, and S. Ciliberto, “Heat fluctuations in a nonequilibrium bath,” *Phys. Rev. Lett.* **106**, 200602 (2011).
- [10] S. Ciliberto, A. Imparato, A. Naert, and M. Tanase, “Heat flux and entropy produced by thermal fluctuations,” *Phys. Rev. Lett.* **110**, 180601 (2013).
- [11] J. P. Pekola, “Towards quantum thermodynamics in electronic circuits,” *Nat. Phys.* **11**, 118–123 (2015).
- [12] K. Hayashi, H. Ueno, R. Iino, and H. Noji, “Fluctuation theorem applied to F<sub>1</sub>-ATPase,” *Phys. Rev. Lett.* **104**, 218103 (2010).
- [13] K. Feitosa and N. Menon, “Fluidized granular medium as an instance of the fluctuation theorem,” *Phys. Rev. Lett.* **92**, 164301 (2004).
- [14] N. Kumar, S. Ramaswamy, and A. K. Sood, “Symmetry properties of the large-deviation function of the velocity of a self-propelled polar particle,” *Phys. Rev. Lett.* **106**, 118001 (2011).
- [15] S. Joubaud, D. Lohse, and D. van der Meer, “Fluctuation theorems for an asymmetric rotor in a granular gas,” *Phys. Rev. Lett.* **108**, 210604 (2012).
- [16] D. Andrieux and P. Gaspard, “A fluctuation theorem for currents and non-linear response coefficients,” *J. Stat. Mech.* P02006 (2007).
- [17] A. C. Barato and U. Seifert, “Thermodynamic uncertainty relation for biomolecular processes,” *Phys. Rev. Lett.* **114**, 158101 (2015).
- [18] A. C. Barato and U. Seifert, “Universal bound on the fano factor in enzyme kinetics,” *J. Phys. Chem. B* **119**, 6555–6561 (2015).
- [19] A. C. Barato and U. Seifert, “Skewness and kurtosis in statistical kinetics,” *Phys. Rev. Lett.* **115**, 188103 (2015).
- [20] R. S. Ellis, *Entropy, Large Deviations, and Statistical Mechanics* (Springer-Verlag, Berlin, 2006).
- [21] H. Touchette, “The large deviation approach to statistical mechanics,” *Phys. Rep.* **478**, 1–69 (2009).
- [22] L. Bertini, A. De Sole, D. Gabrielli, G. Jona-Lasinio, and C. Landim, “Fluctuations in stationary nonequilibrium states of irreversible processes,” *Phys. Rev. Lett.* **87**, 040601 (2001).
- [23] L. Bertini, A. De Sole, D. Gabrielli, G. Jona-Lasinio, and C. Landim, “Macroscopic fluctuation theory for stationary non-equilibrium states,” *J. Stat. Phys.* **107**, 635–675 (2002).
- [24] L. Bertini, A. De Sole, D. Gabrielli, G. Jona-Lasinio, and C. Landim, “Macroscopic fluctuation theory,” *Rev. Mod. Phys.* **87**, 593–636 (2015).
- [25] T. Bodineau and B. Derrida, “Current fluctuations in nonequilibrium diffusive systems: An additivity principle,” *Phys. Rev. Lett.* **92**, 180601 (2004).
- [26] B. Derrida, “Non-equilibrium steady states: fluctuations and large deviations of the density and of the current,” *J. Stat. Mech.* P07023 (2007).
- [27] P. I. Hurtado and P. L. Garrido, “Test of the additivity principle for current fluctuations in a model of heat conduction,” *Phys. Rev. Lett.* **102**, 250601 (2009).
- [28] P. I. Hurtado and P. L. Garrido, “Large fluctuations of the macroscopic current in diffusive systems: A numerical test of the additivity principle,” *Phys. Rev. E* **81**, 041102 (2010).
- [29] M. Gorissen and C. Vanderzande, “Current fluctuations in the weakly asymmetric exclusion process with open boundaries,” *Phys. Rev. E* **86**, 051114 (2012).
- [30] J. Schnakenberg, “Network theory of microscopic and macroscopic behavior of master equation systems,” *Rev. Mod. Phys.* **48**, 571 (1976).
- [31] A. C. Barato and R. Chétrite, “On the symmetry of current probability distributions in jump processes,” *J. Phys. A: Math. Theor.* **45**, 485002 (2012).
- [32] Z. Koza, “General technique of calculating the drift velocity and diffusion coefficient in arbitrary periodic systems,” *J. Phys. A: Math. Gen.* **32**, 7637 (1999).
- [33] R. Chétrite and H. Touchette, “Nonequilibrium microcanonical and canonical ensembles and their equivalence,” *Phys. Rev. Lett.* **111**, 120601 (2013).
- [34] A. C. Barato, R. Chétrite, H. Hinrichsen, and D. Mukamel, “Entropy production and fluctuation relations for a KPZ interface,” *J. Stat. Mech.* P10008 (2010).
- [35] A. C. Barato, R. Chétrite, H. Hinrichsen, and D. Mukamel, “A Gallavotti-Cohen-Evans-Morriss like symmetry for a class of Markov jump processes,” *J. Stat. Phys.* **146**, 294–313 (2012).

- [36] See Supplementary Material of Ref. [17].
- [37] J. Mehl, T. Speck, and U. Seifert, “Large deviation function for entropy production in driven one-dimensional systems,” *Phys. Rev. E* **78**, 011123 (2008).
- [38] S. Dorosz and M. Pleimling, “Entropy production in the nonequilibrium steady states of interacting many-body systems,” *Phys. Rev. E* **83**, 031107 (2011).
- [39] T. Speck, A. Engel, and U. Seifert, “The large deviation function for entropy production: the optimal trajectory and the role of fluctuations,” *J. Stat. Mech.* P12001 (2012).
- [40] E. Roldan and J. M. R. Parrondo, “Estimating dissipation from single stationary trajectories,” *Phys. Rev. Lett.* **105**, 150607 (2010).
- [41] E. Roldan and J. M. R. Parrondo, “Entropy production and Kullback-Leibler divergence between stationary trajectories of discrete systems,” *Phys. Rev. E* **85**, 031129 (2012).
- [42] J. R. Moffitt and C. Bustamante, “Extracting signal from noise: kinetic mechanisms from a michaelis-menten-like expression for enzymatic fluctuations,” *FEBS J.* **281**, 498–517 (2014).
- [43] M. Baiesi, C. Maes, and B. Wynants, “Fluctuations and response of nonequilibrium states,” *Phys. Rev. Lett.* **103**, 010602 (2009).
- [44] R. B. Bapat and T. E. S. Raghavan, *Nonnegative Matrices and Applications* (Cambridge University Press, Cambridge, England, 1997).
- [45] P. I. Hurtado and P. L. Garrido, “Spontaneous Symmetry Breaking at the Fluctuating Level,” *Phys. Rev. Lett.* **107**, 180601 (2011).
- [46] T. R. Gingrich, J. M. Horowitz, N. Perunov, and J. L. England, “Dissipation bounds all steady-state current fluctuations,” *Phys. Rev. Lett.* **116**, 120601 (2016).